AN ANALYTICAL MODEL FOR PIEZOELECTRIC UNIMORPH CANTILEVER SUBJECTED TO AN IMPULSE LOAD

By

ABHINAV ANANT ATHAVALE

A thesis submitted to the

Graduate School-New Brunswick

Rutgers, the State University of New Jersey

In partial fulfillment of the requirements

For the degree of

Master of Science

Graduate Program in Mechanical and Aerospace Engineering

Written under the direction of

KIMBERLY COOK-CHENNAULT

And approved by

_____

_____

_____

_____

New Brunswick, New Jersey

May, 2015

ABSTRACT OF THE THESIS

An Analytical Model of Cantilever Unimorph Acted Upon by an Impulse Load

By Abhinav A Athavale

THESIS Director:

Dr. Kimberly Cook-Chennault

Researchers have been studying ways to harvest various ambient vibrations using piezoelectric materials to power wireless sensors and portable electronics. Literature review includes several such analytical models to harvest energy from vibrations due to the harmonic base excitation using piezoelectric beams. These models have not explored non-harmonic forcing terms independent of frequency such as an impulse load. Presented in this thesis is an analytical model that provides exact solutions for electrical and mechanical response of a piezoelectric unimorph cantilever beam acted upon by an impulse load at the free end. The beam is modeled using the Euler-Bernoulli assumptions. The impulse load is simulated using the delta function. Damping in the form of strain rate damping and viscous damping is taken into consideration for accurate modeling. This model can also capable of obtaining solutions for the conventional forcing terms which have been previously mentioned in the literature review. Closed form expressions for tip displacement of the beam and voltage generated across a load resistance are derived. These closed form expressions are solved using MATLAB to obtain the instantaneous values for

the tip displacement and voltage generated. These instantaneous values for different load resistances are plotted as a function time using MATLAB for better visual perspective. The energy generated by harvester and the mechanical efficiency are found. From the plots it can be inferred that the particular harvester was suited for load resistances between the values of 100 Ω to 1 KΩ. The model is thus used to predict the response of a particular configuration for a piezoelectric unimorph cantilever beam harvester which satisfies the Euler-Bernoulli assumptions and is subjected to impulse loading.

Dedications

In memory of Nirmala Yadav, for her limitless support and selfless love, rest in peace ninna…

Acknowledgements

I thank my advisor Dr. Kimberly Cook-Chennault for her support, guidance, and encouragement during the course of completion of this thesis. This thesis would not have been possible without her investing her patience and efforts in the researcher within me. Her guidance has helped me evolve professionally as an engineer and a researcher; it will surely help me in my career ahead.

I thank the committee members Dr. Haim Baruh and Dr. Aaron Mazzeo for their valuable inputs for improving my thesis. I thank Dr. Haym Benaroya from the MAE department and Dr. Avy Soffer from the Math department for their guidance during the research work. I also thank the Mechanical and Aerospace Engineering Department, Rutgers University for providing such wonderful opportunities and facilities to perform research. I am grateful to the previous researchers for their in this field of research before me.

The members of the Hybrid Energy Systems have supported me immensely during the completion of the research work. I thank Dr. Sankha Banerjee, Udhay Sundar, Wanlin Du, Eric Brickford, Andrew Tang, James Palmer and Ray Wan for their support and help during various stages of this thesis.

I thank my friend for helping me prepare myself for the thesis presentation. Lastly, I thank my family back home in India for their support to make me capable enough to perform and complete such research work. I am grateful for everything they have done for me over all these years.

Thank you,

Abhinav Athavale,

April, 2015

Table of Contents

List of Tables

List of Figures

Nomenclature

T	Stress component
S	Strain component
E	Electric field component
D	Electric displacement component
s	elastic compliance
ε	dielectric constant
d	piezoelectric strain constant
E superscript	evaluated at constant electric field
T superscript	evaluated at constant stress
s superscript	evaluated at constant strain
Y	Young's modulus of material
s subscript	substrate material
p subscript	piezoelectric material
t	thickness of the harvester beam in Y – direction
b	width of harvester beam in Z – direction
w	Transverse beam displacement
m	mass per length of the beam
c_a	viscous air damping coefficient
c_s	strain-rate damping coefficient
γ	Electromagnetic coupling term
v	voltage generated
H	Heaviside function
δ	Delta function
$\phi(x)$	Mass normalized Eigen functions
$\eta(t)$	Modal functions

r subscript	frequency mode
β	Dimensionless Eigen value numbers
ω	Undamped frequency in rad/sec
d subscript	damped frequency in rad/sec
χ	Modal coupling term
ξ	Damping ratios
q	Electric charge
R_L	Load resistance connected across the harvester
τ_c	Electrical circuit time constant

Chapter 1.

1 Introduction

1.1 Research Motivation

Use of wireless portable electronics such as smart phones, tablets, cameras and laptops has burgeoned over the last decade [5]. The growth in device usage may be attributed to the enhancement of their functionality, e.g. mobile web browsing, e-readers for digital documents, downloadable apps, hand writing recognition, touch screens, and network access. The complexity of device functionality and increases in device usage have led to an increase in their power consumption. The majority of these devices are powered by secondary batteries, which comprise large portions of the device's mass and volume, and require frequent charging after minimal usage. As a result of these usage limitations, researchers have begun to investigate power/energy management strategies to minimize power consumption[6-8]; hybrid energy systems; and alternative energy scavenging techniques, to extend the operation time of these portable electronics. Harvesting energy from ambient static and dynamic mechanical loads using piezoelectric materials has become an area of focus, as these devices may be coupled with batteries or used independently to power portable electronics [2, 9]. Mathematical models that predict the electrical output from piezoelectric energy harvesting devices are important for understanding the role(s) these devices may play in the future of powering portable electronics [10-12]. The majority of the existing mathematical models focus on harmonic

base excitation of a cantilevered piezoelectric unimorph beam harvester [9, 13-15]. The work herein focuses on a less-investigated loading condition - impulse loading on the free end of the cantilever beam harvester. This type of mathematical model is appropriate for piezoelectric energy harvesting systems that may be used in devices such as tablets, smart phones, etc. that incorporate touch gesture based technologies.

1.1.1 Growth in use and complexity of portable electronics

The search for alternative strategies for powering portable electronics continues to grow due to rise in the device usage, complexity and utility as seen in the recent studies. For example, the number of mobile phones worldwide is projected to reach 4.77 Billion – nearly 66% of the world population, by 2015 [16]. There are more than eight prominent operating systems available for mobile operating systems and more than 2.5 million apps available for use on a portable devices [17-19]. In addition to consumer devices, the uses of micro-sensors have ventured into the fields of remote communication, health monitoring, biomedical sensing and health care, telecommunication, environmental sensing and industrial monitoring and require reliable and continuous power for extended periods [20].

1.1.2 Power consumption and conventional methods for powering portable electronics

Advances in computing performance and utility of portable electronics have led to increased power usage of the electronics [9]. For example, many smart phones and tablets are now used for online banking, web browsing, online purchases, and social networking. According to Starner T. *et. al.* in [21], the RAM capacity of laptops has increased 256 X times in the past two decades[21], the CPU speed has increased 850 X times in the past two decades [21], while the disk storage capacity has increased 4000 X times in the same period [21]. The additional power usage places more demand on the battery. Batteries do not adhere to Moore's Law [22], and instead are limited in available power, by the inherent specific energy and energy densities of electrochemistry used. The increased power requirements of the electronics has led to a reduction in battery life, thus limiting the functionality of the devices. The disparity between battery size and host device size results from the nonlinear scaling of battery size in comparison with the on-board chip sizes reducing due to the diminishing sizes of transistors. For example, mobile phone batteries account for up to 30-36% of the mass of the entire phone [23]. While demand in computing complexity has increased; the amount of available energy from the battery has increased by only a factor of three [21]. Researchers have looked towards obtaining electrical energy from the ambient mechanical dynamic loading (mechanical energy), to extend the operational life of the device and reduce device volume. This form of energy harvesting may be most suitable for sensors and portable electronics that have power consumption values that can range from a 1μW-10 μW for sensors and up to 100-250 mW for small portable devices such as music players, smart pedometer, smart watches and other wearable electronics [23].

1.2 Piezoelectricity

1.2.1 Definition of Piezoelectricity

A piezoelectric material produces an electrical voltage potential in response to a mechanical stress. Conversely, if an electric voltage potential is applied to a piezoelectric material, it mechanically actuates. This is the converse piezoelectric effect. A material must possess a non-centrosymmetric crystallographic structure in order to be a piezoelectric material. Aluminum nitride and quartz are examples of materials that have non-centrosymmetric structures. On the other hand, some piezoelectric materials exhibit spontaneous polarization due to the separation of negative and positive charge centers in the crystallographic unit cell. The perovskite structure, ABO_3 is a common example of a material that exhibits a spontaneous polarization.

In Figure 1.1, the piezoelectric material, lead-zirconate titanate ($Pb\{Zr_xTi_{1-x}\}O_3$ $(0\leq x\leq 1)$) is presented. Like many piezoelectric materials, PZT has the perovskite structure.

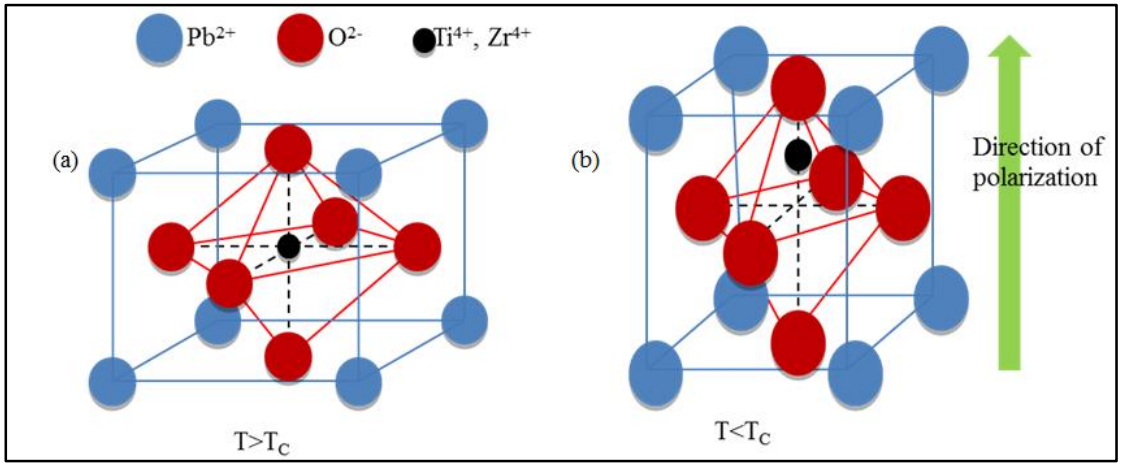

Figure 1:1:Crystal lattice structure of (a) perovskite-type lead zirconate titanate (PZT) unit cell in the symmetric cubic state above the Curie temperature, and the (b) tetragonaly distorted unit cell below the Curie temperature, where the arrow shows the direction of polarization [1].

Each perovskite crystal exhibits a simple cubic symmetry with no dipole moment above a critical temperature (the Curie point) as seen in Figure 1.1.A. At temperatures below the Curie temperature, each crystal has a tetragonal or rhombohedral symmetry and a dipole moment (Figure 1.1 B). Adjoining dipoles form regions of local alignment called domains. These alignments give the domain structure a dipole moment which causes a net polarization. The direction of these polarizations are random as shown in Figure 1.2 A. The domains align themselves when subjected to a strong DC electric field at a temperature slightly higher than the Curie point (Figure 1.2 B), i.e. polarization. During the polarization process, domains most nearly aligned with the electric field expand at the expense of domains that are not aligned with the field, and the element lengthens in the direction of the field. When the electric field is removed most of the dipoles are locked into a configuration of near alignment (Figure 1.2 B). The element now has a permanent polarization, remnant polarization, and is permanently elongated [24].

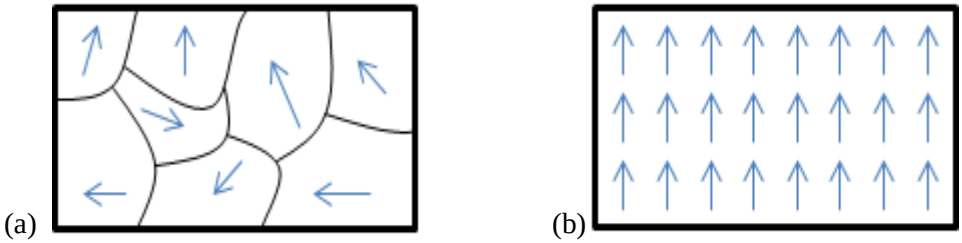

Figure 1.2.Polorizing (poling) of piezoelectric ceramic. (a) Domains arranged in random directions. (b) Domains aligned in direction of the applied electric field[1].

1.2.2 History of Piezoelectricity

Pierre and Jacques Curie first co-authored a publication in 1880 that described a phenomenon where crystals such as tourmaline, quartz, topaz, cane sugar and Rochelle

salt displayed surface charges when mechanically stressed. The expression "piezoelectricity" was coined to distinguish this phenomenon from other related phenomenon like contact electricity and pyroelectricity [25]. The Curie brothers are thus credited for the discovery of piezoelectricity. The converse piezoelectric effect was mathematically deduced according to the laws of thermodynamics by Gabriel Lippmann in 1881. The converse piezoelectric effect was experimentally confirmed by the Curie brothers in 1881 [20].

1.3 Survey of Relevant Literature

1.3.1 Vibration based energy harvesting

Conversion of mechanical vibrations into electrical energy has been studied by several researchers such as Glynne-Jones[26], Mitcheson *et al.* [27], Kornbluh *et al.* [28], and Roundy S. *et al.* [29]. In theory, electrical power derived from mechanical vibration energy could be a potential source of power for sensors and wireless electronics in a wide variety of applications. Many environments experience mechanical vibration, and this mechanical energy can be harvested and converted into electrical energy. In Table 1.1 [2] a list of acceleration magnitude and frequency of potential sources of vibration generally found among common devices is presented.

Table 1.1. Acceleration magnitude and frequency of sources of vibration among commercially available devices [2].

Vibration Source	Acceleration ($m\ s^{-2}$)	Frequency peak (Hz)
Car Engine Compartment	12	200
Base of 3-axis machine tool	10	70
Person tapping their heel	3	1
Car instrument panel	3	13
Door frame just after door closes	3	125
CD on notebook computer	0.6	75
HVAC vent in office building	0.2-1.5	60

Prominent methods for harvesting energy from mechanical vibrations include: electromagnetic induction (Glynne-Jones [26]), electrostatic generation (Mitcheson *et al.* [27]), dielectric elastomers (Kornbluh *et al.* [28]) and piezoelectric materials (Roundy S. *et al.* [29]). A thorough review of forms of piezoelectric energy harvesting is discussed in review articles by Cook-Chennault *et al.* in [23] and by Anton S. and Sodano H. in[9].

Figure 1.3, shows a comparison of the power densities and voltages produced by piezoelectric devices and other common regenerative and lithium-ion power supplies.

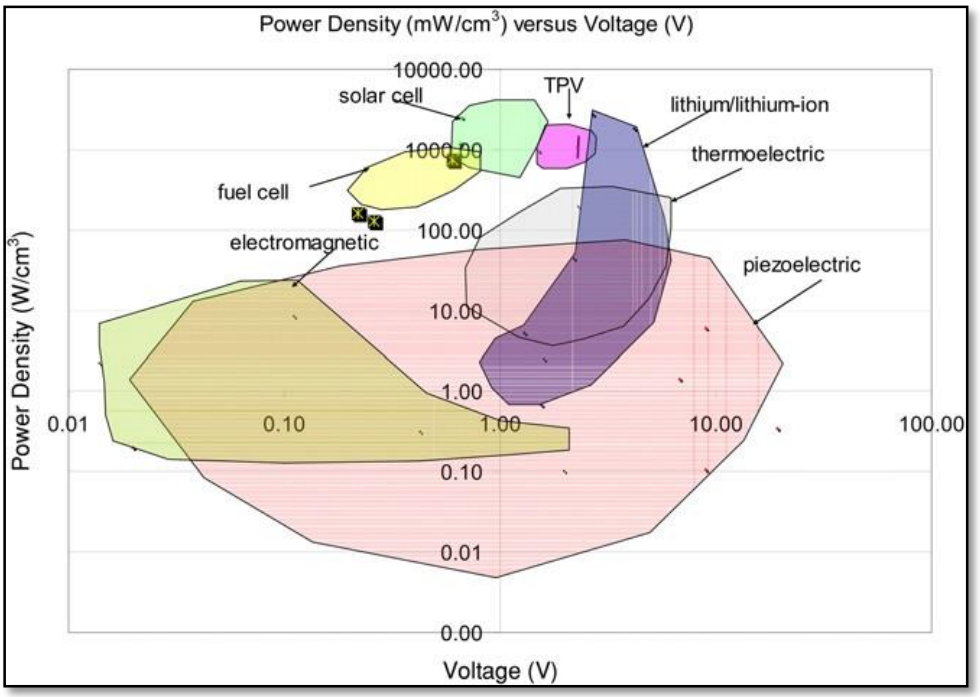

Figure 1.3: Plot of power density versus voltage for common regenerative and lithium/ lithium-ion power supply strategies from Cook-Chennault et al.[2].

Within the category of mechanical to electrical direct energy conversion devices, piezoelectric are of interest because they require no input voltage and can have power density values that are comparable to thin film lithium cells and thermoelectric devices. On the other hand, electromagnetic energy harvesters generally render lower output voltage values, and require post processing in order to achieve a voltage level that can charge a storage device. Also, electrostatic energy harvesters require an input charge to create an alternating electrical output. Due to these reasons piezoelectric energy harvesters have received lot of attention over the last decade.

1.3.2 Loading configurations of piezoelectric materials

Piezoelectric materials produce an electric current when subjected to mechanical loads. The voltage and current produced depend on the properties of the piezoelectric material, as well as, the loading and the structure of the device. The unimorph structure is the focus of this work. A unimorph is comprised of a piezoelectric material that is sandwiched between two electrodes. Two metallic layers that are bonded to the top and bottom surfaces of the piezoelectric material. The electrically conductive layers are used to improve its structural properties of the unimorph and provide a surface for attachment of leads. The most common mounting configuration for a unimorph is a cantilever. The loading experienced by this type of beam structure may be described in terms of modes, e.g. 33 and 31, as illustrated in Figures 1.4 (a) and (b)[23].

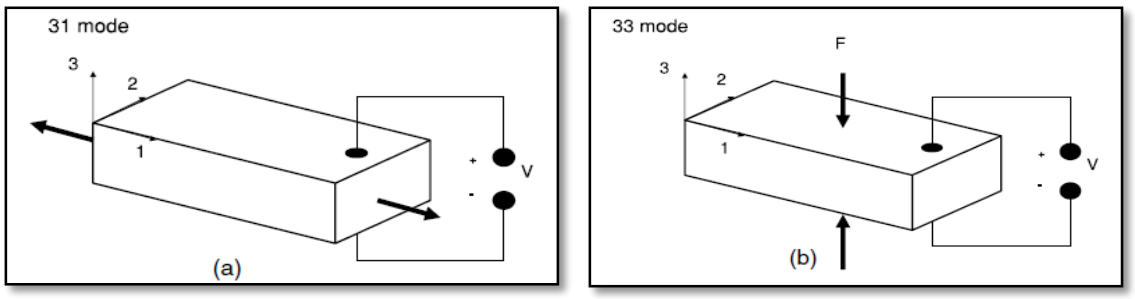

Figure 1.4: Modes of operation for piezoelectric beams, (a) 31-mode of loading for piezoelectric structures, which means the voltage acts in the 3 direction and the mechanical stress acts in the 1 direction and (b) 33-mode of loading for piezoelectric structures which means that both the voltage and the stress act in the same 3 direction. [29].

In Figure 1.4, 1, 2 and 3 represent the x, y, and z directions respectively. The operation of the device in 33-mode means that voltage and stress both act in the z direction. On the other hand, operation of the device in the 31-mode means that the voltage acts parallel to the z axis, while stress is generated along the x axis. Since the coupling factor of the 33-mode is higher than 31-mode, the 33-mode can achieve higher

voltage potential and stress. However, for a very low pressure source and limited device size, the 31-mode conversion may be more suitable for energy harvesting, since larger strains can be produced with smaller input forces with 31 loading [23].

Piezo-ceramic materials are transversely isotropic materials. According to the IEEE Standard on Piezoelectricity [30], the piezoelectric constitutive equations can be used to describe the relationship between the stress (T_{ij}), the strain (S_{ij}), the electric field (E_k) and the electric displacement (D_k) of the material. As such, the tensor forms of the piezoelectric constitutive equations are expressed as:

$$S_{ij} = s^E_{ijkl} T_{kl} + d_{kij} E_k \tag{1.1}$$

$$D_i = d_{ikl} T_{kl} + \varepsilon^T_{ik} E_k. \tag{1.2}$$

In Equations (1.1) and (1.2), s^E, ε^T and d represent the elastic compliance at constant electric field, dielectric constant at a constant stress, and piezoelectric strain coefficient. Superscripts E and T represent constants that are evaluated at constant electric field and constant stress respectively. Electromechanical coefficients such as s, d and ε establish a coupling relation between the direction of the applied mechanical or electrical excitation, and the direction of the response. The piezoelectric strain coefficient, d_{ij} (i= 1, 2, 3, j = 1, 2,…, 6) can be defined as the polarization generated per unit mechanical stress applied to the piezoelectric material or alternatively; the mechanical strain induced per unit electric field applied to the material.

In this thesis, the analytical model is based on Euler-Bernoulli beam theory, where the energy harvester is modeled as a thin beam. The plane stress assumption of the Euler-

Bernoulli beam theory neglects the stress components in all other directions apart from the axial direction [31].

1.3.3 Analytical Models for Prediction of Piezoelectric Performance

Most analytical models presented by researchers over the last decade have focused on prediction of mechanical and electrical performance of cantilevered unimorph or bimorph harvesters subjected to sinusoidal (vibration) mechanical loads. Researchers have studied various types of loading conditions to understand their performance of the harvesters under different circumstances. For example, piezoelectric beams subjected to static [12], torsion and twisting [32], and transverse motion of the clamped base [4] have been investigated to understand the piezoelectric response of the beam element.

For this work, a cantilevered beam such as the one depicted in Figure 1.5, is modeled, wherein strain induced in the piezoelectric (from an applied mechanical load) results in a voltage potential. Beams with this configuration may render energy when the output voltage signal (of variable polarity) is rectified through a bridge rectifier (to produce pulsed direct current). A stable (smoothened) voltage potential may be subsequently achieved via a reservoir capacitor. The processed signal may then be used to charge a secondary battery [20].

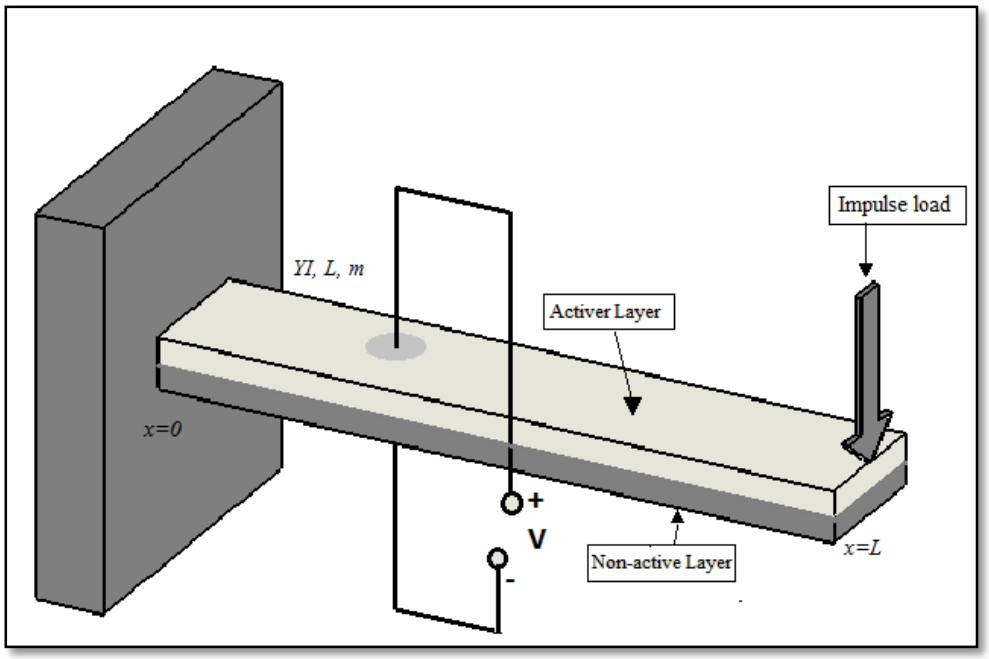

Figure 1.5: Basic input-output principle of piezoelectric energy generators [32].

1.3.4 Literature review of mathematical models of piezoelectric energy harvesters

A comprehensive mathematical model should be sophisticated enough to represent the phenomena as closely as possible and predict its dynamic behavior, yet it needs to be as simple as possible for comprehension and customizations. Several researchers such as [29, 33] have used the lumped parameter approach to model the coupled system dynamics of piezoelectric harvesters. The lumped parameter is a system in which the dependent variables are assumed to be the function of time alone [31]. For example, Neiss S. modeled a non-linear piezoelectric energy harvester that included a mass on the tip of the beam in [33]. The harvester was modeled as a spring-damper system where energy from the oscillating beam is converted to electrical energy. The model was

used to obtain expressions to predict the voltage generated and the power output achieved from the conversion of mechanical energy to electrical energy. The lumped parameter model is an approximation limited to single vibration mode and it neglects electro-mechanical coupling found in the piezoelectric materials.

Gao X. *et al.* [12] studied the voltage developed in a cantilever unimorph beam while varying the length of the non-active layer with respect to the active layer. In this model, the unimorph beam was subjected to a concentrated point load using a load cell. The load applied was static i.e. not varying with time. Maximum displacement of the beam tip and the maximum voltage generated were derived. The maximum induced voltage per unit tip displacement under constant tip displacement conditions, was exhibited when the SS/PZT length ratio was unity. A. Abdelkefi *et al*.[32], also modeled a PZT-steel cantilever beam with asymmetric tip-masses to predict the behavior of these beams when subjected to bending and torsion. In this work, exact solutions for the tip deflection, twisting angle, voltage output and harvested electrical power were derived. Wang [34] developed an analytical model for a curved beam to harvest acoustic energy. This model predicted the voltage and power generated. Energy harvesting using a circular membrane under pressure loading has been investigated by Mo C. *et al*. in [35]. They developed an analytical model to simulate the energy generated by a circular PVDF membrane harvester subjected to transverse deflections. Closed form steady-state response expressions for a thin plate piezoelectric harvester have also been developed by Aridogan U. *et al*. in[36].

Lumentut M.F. and Howard I.M. [37] developed closed form expressions for the tip displacement, voltage generated and power output of a piezoelectric bimorph beam with a mass at its tip. The governing equations were derived using the weak form of Hamiltonian principle to obtain the constitutive equations. Researchers have also looked into analytical modeling of bimorph and multilayer piezoelectric cantilever in the work of Yuan Y. *et al*.[38]. In order to obtain the analytical expressions to predict the voltage generated and tip displacement Erturk A. and Inman D.[4] used Euler-Bernoulli beam theory.

Erturk A. and Inman D.J. [4], Aridogan U. *et al*. [36] and Hosseini S. *et al*.[39] developed models for beams that were excited by the motion of the base. Gao X. *et al*. [12] modeled a unimorph beam that was subjected to a concentrated force. In this work, the concentrated force was generated using a load that was another unimorph piezoelectric cantilever beam. In the work of Abdelkefi A. *et al*.[32], the beam was subjected to coupled bending- torsion vibrations created by placing two masses asymmetrically at the tip of the beam causing an offset between the beam's center of gravity and shear center.

The causes of excitation in all of the aforementioned work could be included into a mathematical model as exponential functions, which were frequency and time dependent. Umeda M. *et al*. in [40], investigated beams subjected to low-frequency sources, wherein excitation was due to an impact load. In this work, experimental studied were conducted to understand the electric power generation produced from a circular transducer subjected to impact load. Pozzi M. [41] presented a model for a bimorph under

impulse loading using dimensionless analysis. The impulse load was a simulated in the model using the Gausian function. In practical applications, the excitation may or may not be a simple harmonic, and easy to solve mathematically.

In this work, the force acting on the beam is an impulse load acting on the free end of the unimorph cantilever beam. The damping mechanisms taken into consideration are viscous air damping and internal strain-rate damping in order to simulate a practical environment as closely as possible. The solution was obtained using separation of variables to obtain closed form expressions for the tip displacement, voltage, current and power for a specified support and loading conditions. This work focuses on generation of a generalized form of excitation force that is independent of frequency.

The model presented in the following chapter is a cantilever piezoelectric energy harvester solved for the transverse vibration using the Euler-Bernoulli beam assumptions. The fundamental assumption of this theory is that deformation due to shear across the section is not taken into consideration, i.e. no shear deformation. A parametrized model is chosen over a single degree of freedom (SDOF) model to obtain the exact solutions for better accuracy as shown in by Erturk A. and Inman D.J. in [4]. Damping mechanisms in the form of viscous damping due to air and internal strain-rate damping (Kelvin-Voigt damping) have been taken into consideration. The harvester is excited by an impulse load that acts on the tip of the free end. Closed form expressions for voltage and mechanical response, i.e. beam deflection are presented. The expressions are then plotted as a function of time using MATLAB to verify the nature of the output obtained from the expressions.

1.4 Thesis Organization

The organization of this thesis is described herein. In Chapter 2, the analytical model formulated for predicting the response of the unimorph cantilever beam subjected to an impulse load at the free end is developed. Closed forms solutions for the electrical and mechanical responses are obtained. In chapter 3 the closed form solutions obtained in Chapter 2 are plotted using MATLAB codes to study the nature of the solution and validate the model. Chapter 4 provides the conclusions drawn from the thesis and a discussion of possible future work.

Chapter 2

2. Analytical Method

The model presented in this chapter describes the method used to predict the mechanical displacement and electrical response (output voltage) of a piezoelectric cantilever beam subjected to an impulse load at the free end. The piezoelectric beam of interest is subjected to a dynamic non-sinusoidal load, which could simulate a touch or a tap on a portable electronic device.

2.1 Beam model description and boundary conditions

This analytical model described here may be used to predict the mechanical and electrical response of the cantilever unimorph beam subjected to an impulse load at its free end. The beam under consideration is modeled as an Euler-Bernoulli beam, and is depicted in Figure 2.1. In Figure 2.1, a unimorph piezoelectric beam is presented, where L, m, and YI represent the length of the beam, mass per unit length of the beam and bending modulus of the composite beam, respectively. The beam is comprised of an active piezoelectric layer and a non-active layer and a perfect bond is assumed between the two layers. The width of the beam is b, as seen in YZ plane. According to [31, 42] an Euler-Bernoulli beam is a long beam made of an isotropic material that is subjected to "pure bending". The cross section of the beam is symmetric to the XY plane as shown in Figure 2.1. The cross-section is rigid in the YZ plane. In this model, it is assumed that the

cross-section of the beam remains plane and normal to the deformed axis of the beam after deformation. Also, the mechanical damping of the beam is expressed as a combination of the internal (strain-rate) and external (air) damping mechanisms.

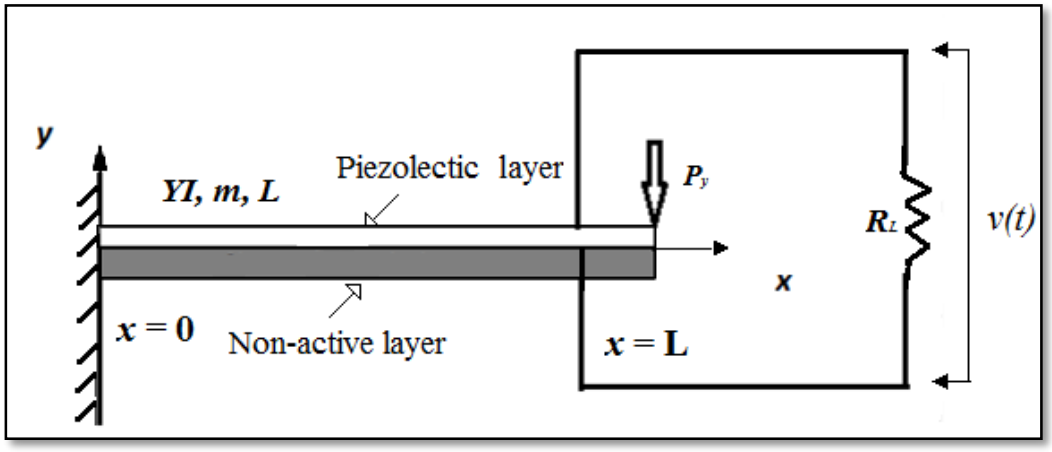

Figure 2.1: A cantilever unimorph beam subjected to an impulse load at the free end. The electrode leads are attached at the top and bottom of the active piezoelectric layer. L is the length of the beam, YI is the bending modulus of the unimorph beam, m is mass per unit length, P_y is the magnitude of the impulse acting on the beam, R_L is the load resistance connected in series with the unimorph harvester beam and v(t) describes the voltage potential generated across the resistive load.

The impulse load, P_y, acts on the free end of the cantilever beam at time $t = 0$ secs. The equation of motion may be obtained by applying Hamilton's Principle to the beam element, which results in an electromechanically coupled differential equation. The differential equation may be solved using separation of variables, to obtain a coupled solution. Decoupled solutions for the electrical output voltage and mechanical displacement are determined with the aid of MATLAB.

2.2 Problem Formulation

2.2.1 Determination of the location of the neutral axis

The neutral axis (NA) of the unimorph is calculated prior to the calculation of the bending

modulus. The cross section of the unimorph is comprised of two different materials; the active piezoelectric and the non-active materials. To locate the neutral axis in the cross section , it is transformed into a cross-section of beam made of one of either material [43]. This technique is often used to find the bending modulus of composite beams such RCC[44]. The purpose of transforming the cross-section is limited to calculating the location of the sectional neutral axis. Figure 2.2 (a) depicts the original beam cross section (prior to transformation). The purpose of the non-active (electrically conductive layer) is to add mechanical strength to the unimorph structure and collect the current generated from the device. The elastic modulus of the non-active layer is higher than the active piezoelectric layer. Hence when the cross section is transformed into a section consisting of only the piezoelectric layer, where the width of the non-active layer is increased by a factor of n, which is the ratio of the elastic moduli of both materials,

$$n = \frac{Y_s}{Y_p}. \tag{2.1}$$

In equation (2.1), Y_s and Y_p represent the elastic Young's moduli for non-active and piezoelectric layers respectively.

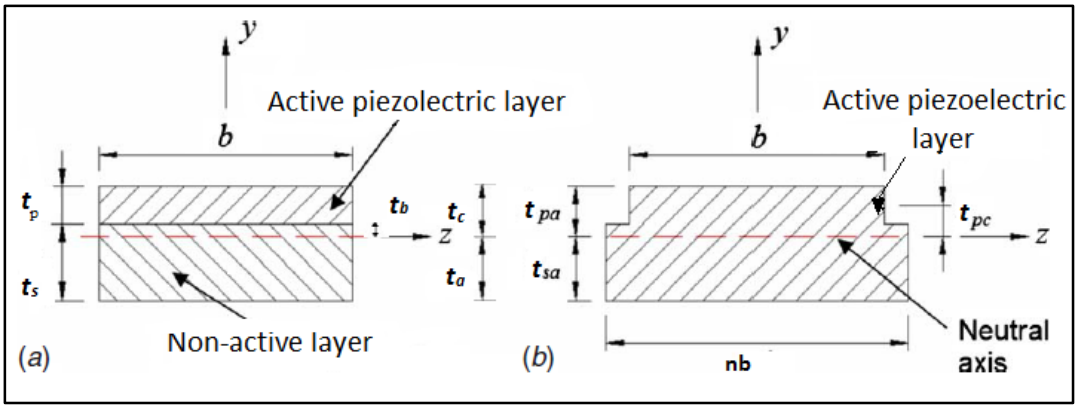

Figure 2.2: (a) The original cross section of the unimorph is for a beam consisting of two materials; piezoelectric and non-active layers and (b) is the converted cross section consisting of only one material, the piezoelectric material [45].

In Figure 2.2 (a) the cross section of the unimorph is presented where t_s, t_p and b represent the distances from the neutral axis to the top and bottom of the beam, and width of the beam, respectively. In Figure 2.2 (b) the equivalent cross section is depicted, which consists of only the active layer. Here, t_{sa} represents the thickness of the layer from the bottom of the non-active layer to the neutral axis. The thickness of the layer from the bottom of the active layer to the neutral axis, t_{sa} is expressed as [20];

$$t_{sa} = \frac{n\,t_s^2+2t_s t_p+t_p^2}{2(nt_s+t_p)}. \tag{2.2}$$

The length from the top of the active layer to the neutral axis, t_{pa}, is expressed as,

The distance from the center of the top layer to the neutral axis, t_{pc} is calculated from,

$$t_{pa} = \frac{n\,t_s^2+2nt_s t_p+t_p^2}{2(nt_s+t_p)}. \tag{2.3}$$

$$t_{pc} = \frac{n\,t_{s(t_p+t_s)}}{2(nt_s+t_p)}. \tag{2.4}$$

The boundaries of the beam are defined with respect to t_a, which is the distance from the bottom of non-active layer to the NA. Also, t_b is the distance from the bottom of the piezoelectric layer (or top of non-active layer) to the NA, and t_c is the distance from top of the piezoelectric layer to the NA. Thus t_a, t_b and t_c are points of location throughout the structure, and are used as integration limits.

$$t_c = t_{pa}, \tag{2.5}$$

$$t_b = t_{pa} - t_p, \tag{2.6}$$

$$t_a = -t_{sa}. \tag{2.7}$$

The internal moments acting on the beam will be evaluated using equations (2.5)-(2.7). In the next section, the differential equation is derived.

2.2.2 Mechanical Equation of Motion with Electrical Coupling

In this section the mechanical equation of motion with electrical coupling is derived. The transverse displacement of any point on the beam along the neutral axis is denoted by $w(x,t)$. If the beam is assumed to be undergoing un-damped free vibration, the equation of motion obtained after application of Newton's second law of motion is [46],

$$YI\frac{\partial w^4(x,t)}{\partial x^4} + m\frac{\partial w^2(x,t)}{\partial t^2} = 0. \tag{2.8}$$

The bending modulus for the composite beam will be derived in the next section. The two types of damping mechanisms included are the viscous air damping and Kelvin-Voigt damping (or strain rate damping). These are prominent mechanisms for damping within an Euler-Bernoulli beam model as discussed by Banks H. and Inman D. in [47]. Viscous air damping is the force acting on the beam due to air particles displaced when the beam is in motion. Strain-rate damping accounts for the structural damping due to frictional internal in the beam [11]. The equation of motion that includes damping effects and a force acting on the beam is expressed as:

$$\frac{\partial^2 M(x,t)}{\partial x^2} + c_s I \frac{\partial^5 w(x,t)}{\partial x^4 \partial t} + c_a \frac{\partial w(x,t)}{\partial t} + m\frac{\partial^2 w(x,t)}{\partial t^2} = f_r(x,t). \qquad (2.9)$$

In equation (2.9) *M and w* are the internal moment acting on the beam and the transverse displacement of beam respectively. The damping coefficients are defined as $c_s I$ for the strain-rate damping and c_a for the viscous air damping, wherein c_s is the equivalent coefficient of strain-rate damping and *I* is the equivalent area moment of inertia.

The same equation can also be derived by applying Newton's Second Law to the beam element, e.g. equating the forces and moment acting on the element with the acceleration due to inertia. A detailed derivation of this equation is available in [46].

The constitutive equations for the isotropic non-active and active piezoelectric structures at constant temperature according to [30] are expressed as:

(for the non-active layer) $$T_{s1} = Y_s S_1 \qquad (2.10)$$

and

(for the active layer) $$S_1 = s_{11}^E T_1 + d_{31} E_3. \tag{2.11}$$

The stress experienced by the active (piezoelectric) layer is,

$$T_{p1} = Y_p (S_1 - d_{31} E_3). \tag{2.12}$$

In equations (2.10) – (2.12), *T*, *S*, *Y*, *d* and *E* are the stress, strain, Young's modulus, piezoelectric constant and electric field respectively. Subscripts *s* and *p* denote properties for the non-active and the piezoelectric layers respectively. s^E_{11} is the elastic compliance at a constant electric field, and is the reciprocal of the Young's modulus.

The internal moment acting on the beam can be obtained by integrating the first moment of the stress distribution over the cross-sectional area,

$$M(x,t) = -\int_{t_a}^{t_b} T_{s1} b\, z\, dz - \int_{t_b}^{t_c} T_{p1} b\, z\, dz. \tag{2.13}$$

Substituting equations (2.10) and (2.12) into equation (2.13) renders,

$$M(x,t) = -\int_{t_a}^{t_b} Y_s\, S_1 b\, z\, dz - \int_{t_b}^{t_c} Y_p (S_1 - d_{31} E_3) b\, z\, dz. \tag{2.14}$$

The bending strain in terms of the radius of curvature of the beam under bending stress is expressed as:

$$S_1 = -z\, \frac{\partial^2 w}{\partial x^2}. \tag{2.15}$$

Following the substitution of equation (2.15) into equation (2.14) and integration, the internal bending moment acting on the cross-section of the beam is,

$$M(x,t) = YI\,\frac{\partial^2 w}{\partial x^2} - \gamma\, v(t), \tag{2.16}$$

where YI is the combined bending modulus of the beam. YI can be determined from,

$$YI = b\left[\frac{Y_s(t_b^3 - t_a^3) + Y_p(t_c^3 - t_b^3)}{3}\right], \tag{2.17}$$

where

$$\gamma = -\frac{Y_p d_{31}(t_c^2 - t_b^2)}{2t_p}. \tag{2.18}$$

The voltage term in equation (2.16) is dependent on constants Y_p, d_{31}, t_c, t_b and t_p. To prevent the elimination of the voltage term during differentiation of equation (2.9), the voltage function is multiplied by a Heaviside step function, $H(x)$ that ranges over the span of the beam.

$$\frac{\partial^2}{\partial x^2}\left(YI\,\frac{\partial^2 w}{\partial x^2} - \gamma\, v(t)\big(H(x) - H(x-L)\big)\right) + c_s I\,\frac{\partial^5 w(x,t)}{\partial x^4 \partial t} + c_a \frac{\partial w(x,t)}{\partial t}$$

$$+ m\frac{\partial^2 w(x,t)}{\partial t^2} = -P_y \delta(x-L)\delta(t). \tag{2.19}$$

Equation (2.19) when simplified, takes the form;

$$YI\frac{\partial^4 w}{\partial x^4} + c_s I\ \frac{\partial^5 w(x,t)}{\partial x^4 \partial t} + c_a \frac{\partial w(x,t)}{\partial t} + m\frac{\partial^2 w(x,t)}{\partial t^2} - \gamma\ v(t)\left[\frac{\partial \delta(x)}{\partial x} - \frac{\partial \delta(x-L)}{\partial x}\right]$$

$$= -P_y \delta(x-L)\delta(t). \tag{2.20}$$

The mechanical equation of motion that includes electrical coupling, equation (2.19), is obtained when equation (2.16) is substituted into equation (2.9). In equation (2.19) and equation (2.20), the term $\left(-P_y\delta(x-L)\delta(t)\right)$ is an impulse load acting at the tip of the beam at time t = 0 seconds.

The general solution for the equation (2.20) is obtained using separation of variables, where it is assumed that the displacement is separated into two parts; one dependent on position and the other on time [48]. The general solution may be expressed as,

$$w(x,t) = \sum_{r=1}^{\infty} \emptyset_r(x)\ \eta_r(t), \tag{2.21}$$

where $\phi_r(x)$ and $\eta_r(t)$ are the mass normalized eigenfunctions and modal coordinates of the cantilevered beam for the rth mode, respectively. Also from [46] we can conclude that for an Euler-Bernoulli beam, the first five terms provide an accurate solution to the differential equation.

According to [47], for proportionately damped systems, the eigenfunctions denoted by $\phi(x)_r$ are the same as the mass normalized eigenfunctions for an un-damped beam undergoing free vibration. These eigenfunctions may be determined from,

$$\phi_r(x) = \sqrt{\left(\frac{1}{mL}\right)}\,[\cosh\beta_r x + \cos\beta_r x + C_r(sinh\beta x - sin\beta x)], \tag{2.22}$$

where β_r describes the range of dimensionless frequency numbers obtained from the characteristic equations:

$$1 + \cosh(\beta_r L)\cos(\beta_r L) = 0 \tag{2.23}$$

and

$$C_r = \frac{sinh\beta_r L - sin\beta_r L}{cosh\beta_r L + cos\beta_r L}. \tag{2.24}$$

The roots of (2.23) may be determined by using the *fzero* function in MATLAB. Hence, the first five values for $\beta_r L$ were determined to be,

$$\beta_r = \begin{Bmatrix} 1.8750 \\ 4.6491 \\ 7.8548 \\ 10.996 \\ 14.1372 \end{Bmatrix} \tag{2.25}$$

The mass normalized eigenfunctions defined in (2.22) must satisfy the orthogonality conditions,

$$\int_{x=0}^{L} m\,\phi_s\phi_r dx = \delta_{rs}, \tag{2.26}$$

and

$$\int_0^L YI\,\phi_s \frac{\partial^4\,\phi_r}{\partial x^4} = \omega_r^2\delta_{rs}\,, \tag{2.27}$$

where δ_{rs} is the Kronecker's delta.

The un-damped natural frequency, ω_r, is expressed as,

$$\omega_r = (\beta_r)^2 \sqrt{\frac{YI}{m}}. \tag{2.28}$$

Equation (2.20) is multiplied by $\phi_s(x)$ and integrated from 0 to L to obtain equation (2.29), which is an electromechanically coupled ordinary differential equation for modal response:

$$\frac{\partial^2 \eta(t)}{\partial t^2} + 2\,\xi_r \omega_r \,\frac{\partial \eta(t)}{\partial t} + \omega_r^2 \eta(t) + \chi_r v(t) = F_r(t) \tag{2.29}$$

where,

$$2\xi_r = \left(\frac{c_s I \omega_r}{2\,YI} + \frac{c_a}{2m\omega_r}\right), \tag{2.30}$$

$$\chi_r = \gamma \left(\frac{d\phi(x)}{dx}\right)_{x=L}',$$

and $$F_r(t) = -P_y(\phi)_{x=L}\,\delta(t).$$

*T*he mechanical damping (strain rate and viscous air-damping) is $2\xi_r$.

*T*he following property is exploited to determine χ_r,

$$\int_{-\infty}^{\infty} \frac{d^n \delta(x - x_0)}{dx^n} \; f(x)dx = (-1)^n \frac{df^n(x_0)}{dx^n}. \tag{2.31}$$

The solution for Equation (2.27) is obtained using Duhamel's principle [46], and expressed as,

$$\eta(t) = \frac{1}{\omega_{d_r}} \int_{\tau=0}^{t} [F_r(\tau) - \chi_r v(\tau)]\, e^{-\xi_r \omega_r (t-\tau)} \sin(\omega_{d_r}\,(t-\tau))\, d\tau, \tag{2.32}$$

where $\omega_{d_r} = \omega_r\sqrt{1-\xi_r^2}$, is the damped natural frequency of the r[th] mode. In equation (2.32), $\eta(t)$ is a function of $v(t)$, which is to be determined.

2.2.3 Coupled Electrical Circuit Equation of a Thin Piezo-ceramic Layer under Dynamic Bending

Just as equation (2.20) is a mechanical equation of motion with electrical coupling, an electrical equation with mechanical coupling can be derived for the circuit described in Figure 2.3 (b) [4]. The constitutive relation for piezoelectric materials is given by,

$$D_3 = d_{31}T_1 + \varepsilon_{33}^T E_3(t), \tag{2.33}$$

where D_3 is the electric displacement and $\varepsilon_{33}^{\mathrm{T}}$ is the permittivity at constant stress[30]. As shown in Equation (2.11), T_1 can be written as:

$$T_1 = Y_p(S_1 - d_{31}E_3),$$

The permittivity is replaced by permittivity at constant strain [30], by substituting equation (2.11) into equation (2.33), the electric displacement expression becomes,

$$D_3 = d_{31}\left(Y_p S_1\right) - \frac{\varepsilon_{33}^S v(t)}{t_p}, \tag{2.34}$$

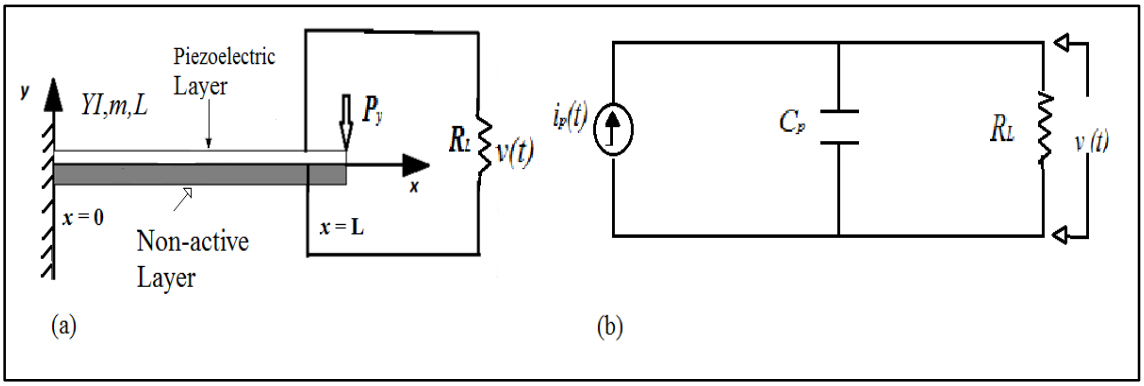

Figure 2.3: (a) Unimorph cantilever connected to a resistive load and (b) Corresponding electrical circuit electrical circuit with piezoelectric capacitance and load resistance.

Equation (2.20) is the mechanical equation of motion with electrical coupling. The electrical equation with mechanical coupling can be derived for the electrical circuit described in Figure 2.3 (b) [4]. The constitutive relation for piezoelectric materials is given by,

$$D_3 = d_{31}T_1 + \varepsilon_{33}^T E_3(t), \tag{2.35}$$

where D_3 is the electric displacement and ε_{33}^T is the permittivity at constant stress [30]. As shown in equation (2.12), T_1 can be written as:

$$T_1 = Y_p(S_1 - d_{31}E_3).$$

The permittivity is replaced by permittivity at constant strain[30], by substituting equation (2.12) into equation (2.35), to render an expression for electric displacement as a function of voltage:

$$D_3 = d_{31}(Y_p S_1) - \frac{\varepsilon_{33}^S v(t)}{t_p}, \tag{2.36}$$

where

$$\varepsilon_{33}^S = \varepsilon_{33}^T - d_{31}^2 Y_p, \tag{2.37}$$

and
$$E_3(t) = -\frac{v(t)}{t_p}. \tag{2.38}$$

The average bending strain can be expressed as a function of t_{pc}, in equation (2.39),

$$S_1(x,t) = = t_{pc}\frac{\partial^2 w}{\partial x^2}. \tag{2.39}$$

Substituting equation (2.40) into equation (2.41) yields:

$$D_3 = = d_{31}Y_p t_{pc}\frac{\partial^2 w}{\partial x^2} - \frac{\varepsilon_{33}^S}{t_p}v(t). \tag{2.40}$$

The electric charge $q(t)$ developed in the piezoelectric layer can be expressed as,

$$q(t) = \int D \cdot n \, dA, \tag{2.41}$$

where *n* is the normal vector and *dA = bdx,* is the electrode area *i.e.* the top section of the beam.

Substitution of equation (2.40) into equation (2.41) yields,

$$q(t) = -\int_0^L b\left(d_{31}Y_p t_{pc}\frac{\partial^2 w}{\partial x^2} + \frac{\varepsilon_{33}^S}{t_p}v(t)b\,L\right)dx\,. \tag{2.42}$$

The current flowing through the circuit is given as,

$$i(t) = \frac{dq(t)}{dt} = -\int_{x=0}^{L} d_{31}Y_p t_{pc}\frac{\partial^3 w}{\partial x^2 \partial t}dx - \frac{\varepsilon_{33}^S}{t_p}\frac{dv(t)}{dt}b\,L. \tag{2.43}$$

From equation (2.43), it is evident that the current generated is due to the vibratory motion of the beam in response to the impulse load. The current generated in the piezoelectric layer can also be expressed using Ohm's law as,

$$i(t) = \frac{v(t)}{R_L}. \tag{2.44}$$

Substituting equation (2.44) back in to equation (2.43) yields,

$$\frac{v(t)}{R_L} = -\int_{x=0}^{L} d_{31} Y_p t_{pc} \frac{\partial^3 w}{\partial x^2 \partial t} dx - \frac{\varepsilon_{33}^S}{t_p} \frac{dv(t)}{dt} b\, L, \tag{2.45}$$

Rearranged, equation (2.45) becomes,

$$\frac{\varepsilon_{33}^S b\, L}{t_p} \frac{dv(t)}{dt} + \frac{v(t)}{R_L} = -\int_0^L b\, d_{31} Y_p t_{pc} \frac{\partial^3 w}{\partial^2 x \partial t} dx. \tag{2.46}$$

Applying Kirchhoff's Law to the electrical circuit shown in Figure 2.3 (b) renders,

$$C_p \frac{d\, v(t)}{dt} + \frac{v(t)}{R_L} - i_p(t) = 0\,. \tag{2.47}$$

The term $\frac{\varepsilon_{33}^S}{t_p} b\, L$ is the capacitance across of the piezoelectric layer. Substitution of equation (2.21) (the series form of solution) into equation (2.46) yields,

$$\frac{dv(t)}{dt} + \frac{v(t)}{\tau_c} = \sum_{r=1}^{\infty} \varphi_r \frac{d\eta_r(t)}{dt}, \tag{2.48}$$

where,

$$\varphi_r = -\frac{d_{31} Y_p t_{pc} t_p}{\varepsilon_{33}^S L} \int_{x=0}^{L} \frac{d^2\, \phi_r(x)}{dx^2} dx \;\; = \frac{d_{31} Y_p t_{pc} t_p}{\varepsilon_{33}^S b\, L} \;\; \left(\frac{d\phi_r(x)}{dx}\right)_{x=L}. \tag{2.49}$$

and

$$\tau_c = \frac{(R_L \varepsilon_{33}^S b\, L)}{t_p}. \tag{2.50}$$

The Leibniz rule for differentiation under integral sign states that,

$$\frac{d}{dx}\left(\int_{f_1(x)}^{f_2(x)} g(t)dt\right) = g[f_2(x)]f_2'(x) - g[f_1(x)]f_1'(x). \quad (2.51)$$

Substituting $\frac{d\eta}{dt}$ into equation (2.51) yields,

	$\frac{d\eta}{dt} = \frac{d}{dt}\int_0^t [F_r(\tau) + \chi_r v(\tau)]\, e^{-\xi_r \omega_r (t-\tau)} \sin\left(\omega_d (t-\tau)\right) d\tau,$	
	$= \int_0^t [F_r(\tau) + \chi_r v(\tau)]\, e^{-\xi_r \omega_r (t-\tau)} (-\xi_r\, \omega_r\, \sin\left(\omega_d (t-\tau) + \omega_d\, cos\left(\omega_d (t-\tau)\right)\right) d\tau.$	(2.52)

Substitution of equation (2.52) into equation (2.51) yields,

$$\frac{dv(t)}{dt} + \frac{v(t)}{\tau_c} = \sum_{r=1}^{\infty} \varphi_r \int_0^t [F_r(\tau) + \chi_r v(\tau)]\, e^{-\xi_r \omega_r (t-\tau)} (-\xi_r\, \omega_r\, \sin\left(\omega_d (t-\tau) + \omega_d\, cos\left(\omega_d (t-\tau)\right)\right) d\tau \quad (2.53)$$

Laplace transforms are used to solve equation (2.53), to obtain a decoupled solution for the voltage function, *v (t)*. The right hand side of equation (2.53) can be viewed as a convolution of the terms (τ) and t. The Laplace transform of a convolution is the product of the Laplace transforms of each individual term. The step-wise procedure for applying Laplace transforms is provided below, where the final expression for V(s) is given in equation (2.54)

$$sV(s) + \frac{1}{\tau_c}V(s) =$$

$$\sum_{r=1}^{\infty} \{ \varphi_r \mathcal{L}\left[-P_y \delta(t)\right] + \chi_r v(t) \mathcal{L}\left[e^{\xi_r \omega_r (t-\tau)} \sin \omega_d (t-\tau)\right], \\ + \chi_r v(t) \mathcal{L}\left[\omega_d \cos \omega_d (t-\tau)\right] \}$$

$$sV(s) + \frac{1}{\tau_c}V(s) = \sum_{r=1}^{\infty} \varphi_r \left[-P_y \phi_{x=L} + \chi_r V(s)\right] \left(\frac{-\xi_r \omega_r \omega_d}{(s+\xi_r \omega_r)^2 + \omega_d^2} + \right.$$

$$\left. \left(\frac{\omega_d (s+\xi_r \omega_r)}{(s+\xi_r \omega_r)^2 + \omega_d^2}\right)\right),$$

$$V(s)\left[s + \frac{1}{\tau_c} - \varphi_r \chi_r \left(\frac{s\omega_d}{(s+\xi_r \omega_r)^2 + \omega_d^2}\right)\right] = \frac{\left(-P_y \phi_{x=L} \varphi_r \omega_d \tau_c s\right)}{\left(s+\xi_{r\omega_r}\right)^2 + \omega_d^2},$$

$$V(s) = \frac{\left(-P_y \varphi_r \phi_{x=L} \chi_r \omega_r \tau_c\right)s}{\tau_c s^3 + (2\xi_r \omega_r \tau_c + 1)s^2 + \left(\tau_c \omega_r^2 + 2\xi_r \omega_r + \chi_r \varphi_r \omega_d \tau_c\right)s + \omega_r^2}. \quad (2.54)$$

In equation (2.45), *a*, *b*, and *c* are designated as roots of the denominator. The roots can be real or complex in nature. A damped vibratory system exhibits an exponential function. Hence, the real parts of the roots must be negative. This can be used as a check to analyze the validity of the expressions obtained later. However, due to the nature of the denominator, the roots have to be obtained numerically by plugging values into MATLAB and using the function- *roots ()*.

The values for T_c, ω_r, ω_d *and* χ_r can be found using the formulae mentioned above. The first five modes are considered for our solution. The value for modal damping ratios

are taken as (*0.010*, *0.013*, *0.033*, *0.064*, *0.106*) from [15] and the damping ratios for the first two modes were determined experimentally in the work of Erturk A. and Inman D.J.[15].. The remaining values are found using equation (2.30). The dimensions of the beam considered are selected from [4], because the damping ratios utilized are from this reference. The properties of the materials of the unimorph are enlisted in Table 2.1 below.

Table2.2: Geometric, material and electromechanical parameters of the beam from [15] .

Length of the beam, L (mm)	100
Width of the beam, b (mm)	20
Thickness of the substructure, t_s (mm)	0.5
Thickness of the PZT, t_p (mm)	0.4
Young's modulus of the substructure, Y_s (GPa)	100
Young's modulus of the PZT, Y_p (GPa)	66
Mass density of the substructure, p_s (kg/m^3)	7165
Mass density of the PZT, p_P (kg/m^3)	7800
Piezoelectric constant, d_{31} (pm/V)	−190
Permittivity, ε_{33}^{S} (nF/m)	15.93

Thus, equation (2.45) can be written as,

$$V(s) = -P_y \omega_d \phi_{x=L} \tau_c \varphi_r \left(\frac{s}{(s-a)(s-b)(s-c)}\right). \quad (2.56)$$

Taking Laplace inverse transform of equation (2.46), renders decoupled closed form expressions for the voltage generated within the piezoelectric layer due to impulse load acting on the tip end of the cantilever beam.

$$v(t) = -P_y \omega_d \phi_{x=L} \tau_c \varphi_r \left(A\, e^{at} + B e^{bt} + C e^{ct}\right), \quad (2.57)$$

where $A = \frac{a}{(a-b)(a-c)}$, $B = -\frac{b}{(a-b)(b-c)}$, $C = \frac{c}{(a-c)(b-c)}$.

Substitution of equation (2.57) into equation (2.32) produces the decoupled solution for the modal response of the unimorph beam,

$$\eta_r(t) = \int_0^t \left(-P_y \phi_{x=L} \delta(\tau) - \chi_r v(\tau)\right) (A e^{a\tau} + B e^{b\tau} + C e^{c\tau})$$

$$e_r^{-\xi_r \omega_r (t-\tau)} \sin(\omega_d (t-\tau) d\tau.$$

Upon integrating this expression, the solution obtained is,

$$\eta_r(t) = -P_y\phi_{x=L}e^{-\xi_r\omega_r t}\sin(\omega_d t) + \chi_r P\phi_{x=L_y}\varphi_r\omega_d\tau_c \left[\left(\frac{A}{(a+\xi_r\omega_r)^2+\omega_d^2}\left(e^{at} + e^{-\xi_r\omega_r t}\left((a+\xi_r\omega_r)sin(\omega_d t) - \omega_d\cos(\omega_d t)\right)\right)\right) + \frac{B}{(b+\xi_r\omega_r)^2+\omega_d^2}\left(e^{bt} + e^{-\xi_r\omega_r t}\left((b+\xi_r\omega_r)sin(\omega_d t) - \omega_d\cos(\omega_d t)\right) + \frac{C}{(c+\xi_r\omega_r)^2+\omega_d^2}\left(e^{ct} + e^{-\xi_r\omega_r t}\left((c+\xi_r\omega_r)sin(\omega_d t) - \omega_d\cos(\omega_d t)\right)\right)\right)\right].$$

(2.58)

The mechanical response of the beam can be obtained by substituting equation (2.21) and equation (2.58) back into the summation term described in equation (2.21). The displacement of the free end can be obtained by substituting *x=L* into the solution.

$$w(L,t) = \sum_{r=1}^{\infty}\emptyset_r(L)\,\eta_r(t).$$

$$w\,(L,t) = \sum_{r=1}^{\infty}\left(\sqrt{\left(\frac{1}{mL}\right)}\,[\cosh\beta_r x + \cos\beta_r x + C_r(sinh\beta x - sin\beta x)]\right)\left(-P_y\phi_{x=L}e^{-\xi_r\omega_r t}\sin(\omega_d t) + \chi_r P\phi_{x=L_y}\varphi_r\omega_d\tau_c \left[\left(\frac{A}{(a+\xi_r\omega_r)^2+\omega_d^2}\left(e^{at} + e^{-\xi_r\omega_r t}\left((a+\xi_r\omega_r)sin(\omega_d t) - \omega_d\cos(\omega_d t)\right)\right)\right) + \frac{B}{(b+\xi_r\omega_r)^2+\omega_d^2}\left(e^{bt} + e^{-\xi_r\omega_r t}\left((b+\xi_r\omega_r)sin(\omega_d t) - \omega_d\cos(\omega_d t)\right) + \frac{C}{(c+\xi_r\omega_r)^2+\omega_d^2}\left(e^{ct} + e^{-\xi_r\omega_r t}\left((c+\xi_r\omega_r)sin(\omega_d t) - \omega_d\cos(\omega_d t)\right)\right)\right)\right]\right).$$

(2.59)

The solution obtained from this derivation is validated in Chapter 3.

Chapter 3

3. Results, Discussion and Model Validation

The closed form solutions for prediction of the output voltage potential and tip displacement (Equations 2.57 and 2.59 respectively) have been developed for an Euler-Bernoulli cantilever beam subjected to a mechanical impulse load at its free end. The solution set to these equations were achieved using a series of MATLAB codes (script developed as part of this thesis is available in Appendix A). The solution set for the tip displacement, $w(L,t)$, voltage generated, $v(t)$, and the power generated, $P(t)$, across a load resistance are plotted as a function of time t (seconds).

The device is assumed to be an Euler-Bernoulli beam. The predictions from the model will be verified and compared to the trends observed in the work of Gao X. *et. al.* [3]. In order to utilize the values of the modal damping ratios for the unimorph which have been previously calculated in the work of Erturk A. *et. al.* [4]; the dimensions of the beam in this thesis are the same as the dimensions of the beam in the work of Erturk A. *et. al.*. In [4], Erturk A. *et. al.* studied the electrical and mechanical response of an unimorph subjected to base excitation at resonant frequencies. The dimensions for the beam used in this study and those for the beam studied by Erturk. *et al.*[4], and are summarized in Table 3.1. The impulse load applied to the tip of the beam is -0.01N and time interval for the impulse was set equal to 1 millisecond.

Table 3.3: Geometric, material and electromagnetic properties of the unimorph cantilever beam in Erturk A. et.al. [4]

Variable	Description (units)	Erturk A. *et al.* *[4]*	This Thesis
L	Length of the beam (mm)	100	100
b	Width of the beam (mm)	20	20
t_s	Thickness of the substructure (mm)	0.5	0.5
t_p	Thickness of the PZT (mm)	0.4	0.4
Y_s	Young's modulus of the non-active layer (GPa)	100	100
Y_p	Young's modulus of the PZT (GPa)	66	66
ρ_s	Mass density of the substructure (kg/m^3)	7165	7165
ρ_p	Mass density of the PZT (kg/m^3)	7800	7800
d_{31}	Piezoelectric constant (pm/V)	−190	−190
ε_{33}^{S}	Permittivity (nF/m)	15.93	15.93

3.1 Tip displacement of the free end of the cantilever beam

The displacement, $w(L,t)$, of the free end of the cantilever beam subjected to an impulse load of -0.01 N, for 1 millisecond (*ms*) is plotted as a function of time in Figure 3.1. . The force acts at time $t = 0$ seconds. The tip reaches the maximum displacement of w

= -0.0134 *m*, and undergoes oscillatory decay, where a displacement equal to 0 is achieved when the time *t*=1 second. The tip displacement profile observed is an exponential decay as a function of time due to viscous damping due to air surrounding the beam and internal strain-rate damping within the beam.

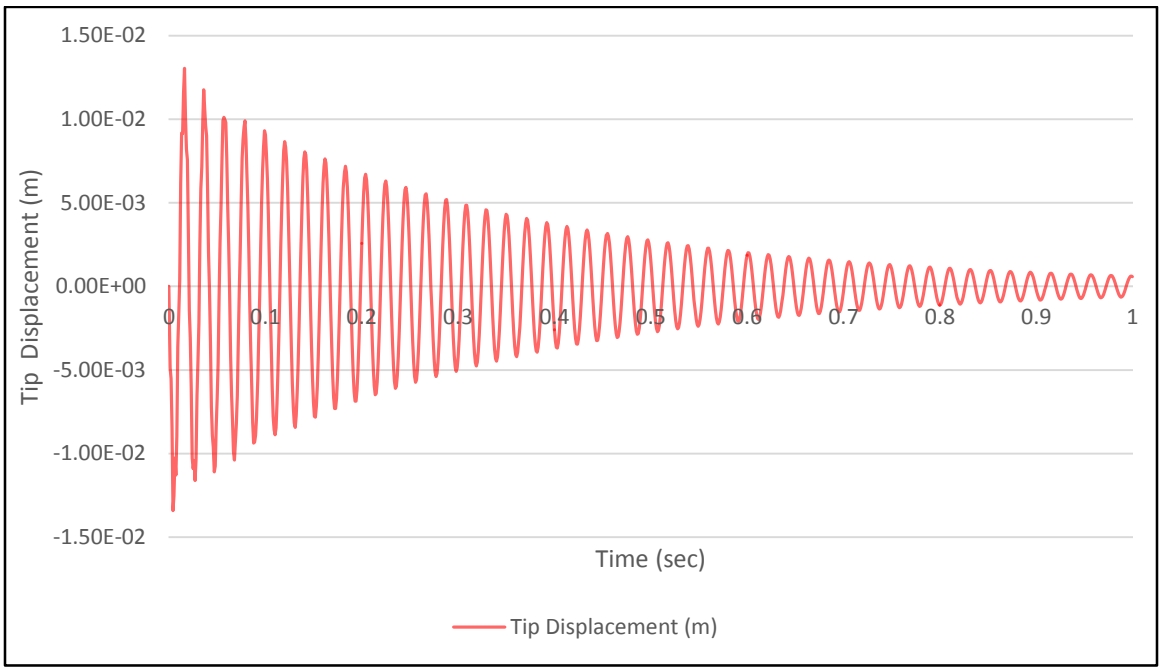

Figure 3.1: Displacement of the free end of the cantilever beam under impulse load.

The displacement trend observed in this work is similar to the trend observed by Gao X. *et. al.* [3] for the tip deflection of a unimorph cantilever. In the work of Gao X. *et. al.* in [3], a concentrated force was applied to the tip of a piezoelectric unimorph cantilever using a load cell., which bends the unimorph beam. The resultant tip displacement and voltage generated were plotted versus time as shown in Figure 3.3. The dimensions of the beam studied by Gao. X. *et. al.* have been enlisted in the table below.

Table 3.4: Geometric, material and electromagnetic properties of the unimorph cantilever beam in Gao X. et. al.[3]

Variable	Description (units)	Gao *et al. [4]*	This Thesis
L	Length of the beam (mm)	12	100
b	Width of the beam (mm)	2.05	20
t_s	Thickness of the substructure (μm)	50	0.5
t_p	Thickness of the PZT (μm)	127	0.4
Y_s	Young's modulus of the non-active layer (GPa)	200	100
Y_p	Young's modulus of the PZT (GPa)	62	66
ρ_s	Mass density of the substructure (kg/m^3)	7900	7165
ρ_P	Mass density of the PZT (kg/m^3)	7800	7800
d_{31}	Piezoelectric constant (pm/V)	−320	−190

The resultant tip displacements for the piezoelectric unimorph cantilever beam were obtained empirically and plotted versus time. As seen in Figure 3.2 after the force was applied at time t = 0 second, the tip displacement increased and reached the peak value of 35 μm at about t=1.7 milliseconds followed by oscillatory decay with time, indicating underdamped transient response. The tip displacement obtained from the analytical model (Figure 3.1) presented in this thesis follows the trends similar to Figure 3.2.

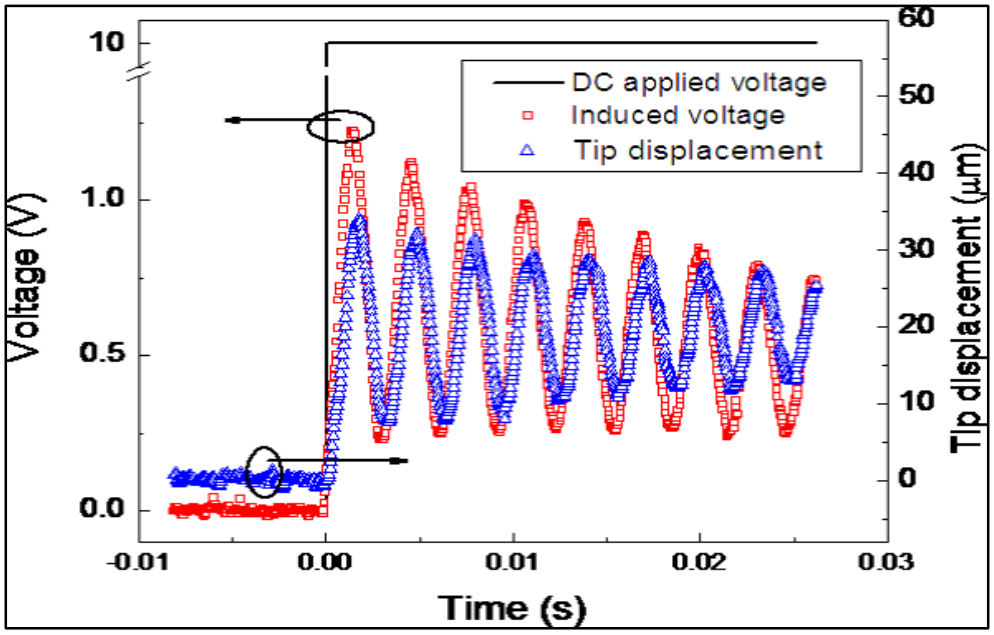

Figure 3.6:Tip displacement and induced voltage versus time of cantilever unimorph when a 10 V DC voltage was applied to the load cell at t = 0 [3].

3.2 Voltage generated across the resistive load

The electrical circuit configuration for the unimorph is shown in Figure 3.3 where the voltage across a resistive load, R_L is used to calculate the output voltage and power generated by the system. In Figure 3.3, C_p represents the internal capacitance of the piezoelectric layer.

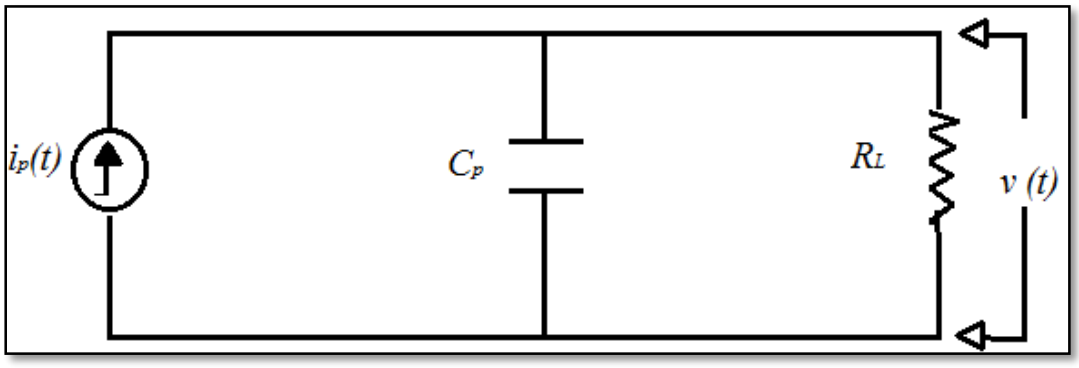

Figure 3.3: Electrical configuration of a unimorph cantilever connected to resistive load[4].

The voltage generated across the resistive load as given by Equation (2.57),

$$v(t) = -P_y \omega_d \phi_{x=L} \tau_c \varphi_r \left(A\, e^{-at} + Be^{-bt} + Ce^{-ct} \right), \tag{3.1}$$

where: $A = \frac{a}{(a-b)(a-c)}$, $B = -\frac{b}{(a-b)(b-c)}$, $C = \frac{c}{(a-c)(b-c)}$.

The voltage generated is exponentially proportional to the roots a, *b*, *c* and time *t* which is a solution set of generated using MATLAB. From equation (2.54) it is seen that the roots *a*, *b* and *c* are dependent upon ω_r , ξ_r , τ_c, χ_r, φ_r. From equations (2.27), (2.30),(2.49) and (2.50) it can be said that ω_r ,ξ_r , τ_c, χ_r, φ_r are dependent on the mass per unit length (*m*), permittivity (ε_{33}^{S}), length (*L*), piezoelectric constant (d_{31}), Young's modulus *Y*, beam thickness, beam width (*b*), and load resistance (R_L).

For a given configuration for the cantilever unimorph, the geometric dimensions of the beam and material properties remain constant, hence the value of ω_r ,ξ_r , χ_r, φ_r remain constant. The value of τ_c is directly proportional to R_L from Equation (2.50). Thus the value of the roots vary with the respect to the load resistance R_L. As the value of load resistance R_L across the circuit increases the values of *a*, *b* and *c* increase. Due to this increase in the exponential power, the value of voltage approaches zero quicker with the increase in R_L. Presented below are plots for the voltage generated across the electrodes when the load resistance connected in the circuit is 100 Ωs (Figure 3.4) and 1 K−Ω (Figure 3.5). The resistance values were selected such as to demonstrate the quicker dampening

of the generated voltage with increase in the resistance values. In Figure 3.4 the maximum voltage generated is 0.0052 Volts, but it is consistent with the tip displacement.

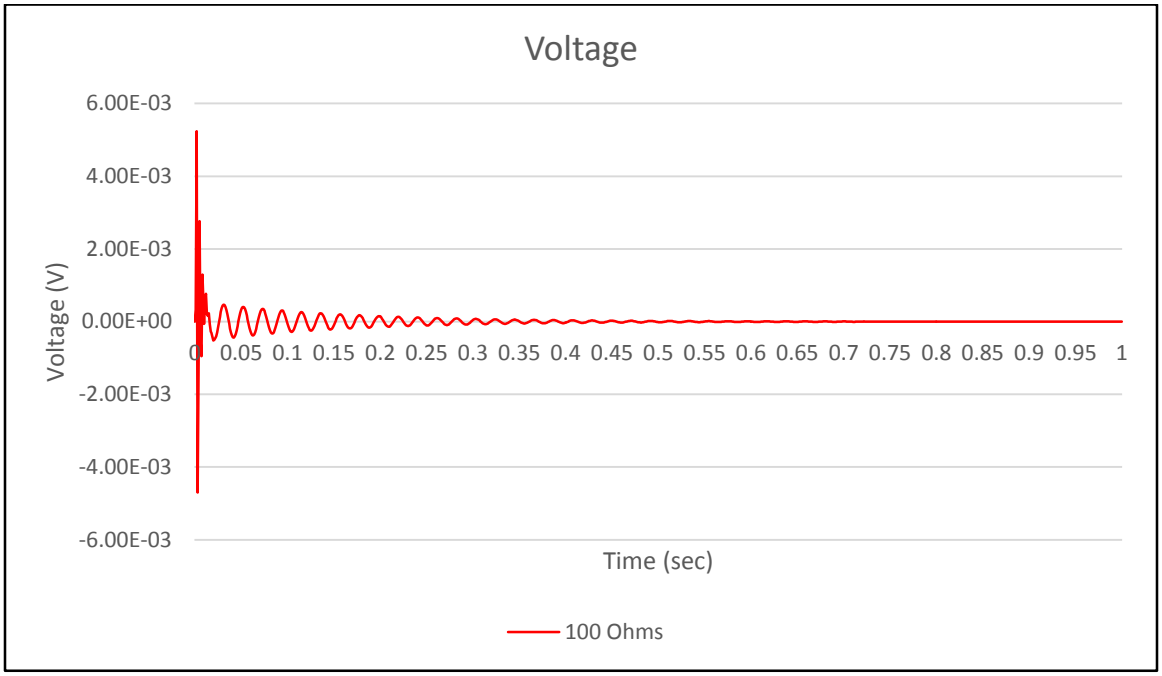

Figure 3.4: Voltage generated across a load resistance of 100 Ohms.

Comparing Figure 3.4 and Figure 3.5, the maximum voltage generated in the later is 0.121 Volts, but the exponential decay to the X axis is quicker. Hence it can be said that with increasing load resistance, the value of the peaks or the maximum load generated increases. But voltage generation quickly dampens down to negligible values.

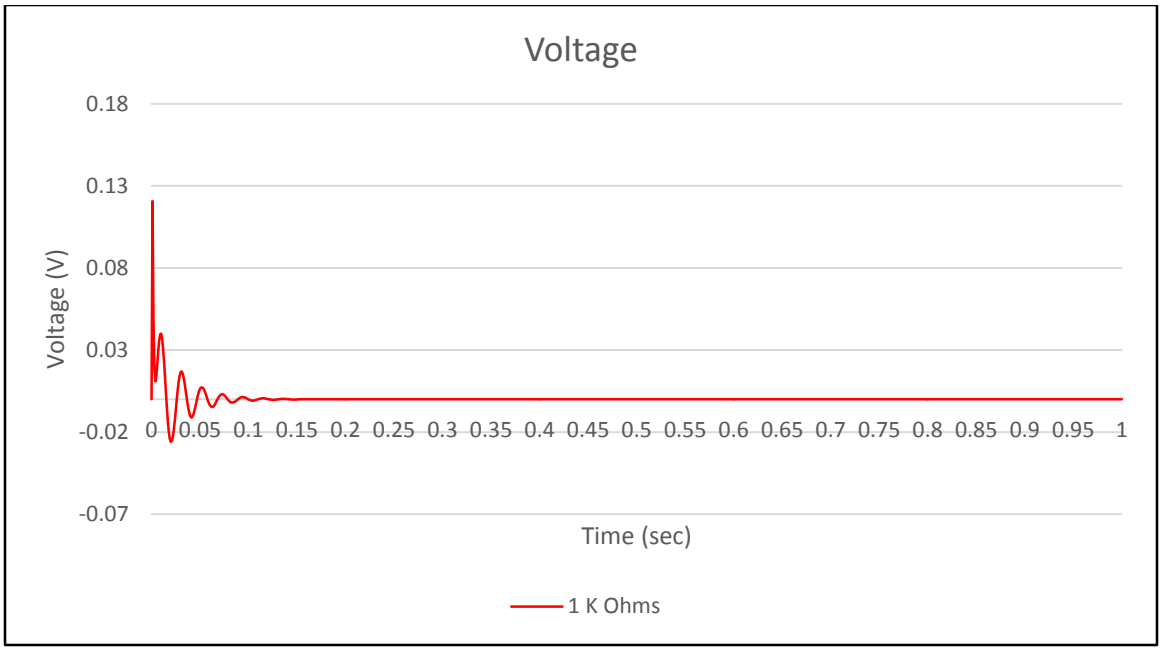

Figure 3.5: Voltage generated across a load resistance of 1K-Ohm.

3.3 Instantaneous current generated through the load

The current flowing through the resistive load is obtain using the Ohm's law $i(t) = v(t)/R_L$. From the previous section the peak voltage generated increases with increase in the load resistance. The current generated increases with the increases in the load resistance. The solution values for instantaneous current are plotted as function of time (Figure 3.6 and 3.7). The peak current flowing through the resistance of 100 Ωs is 52.4 μA (Figure 3.6). While the peak current flowing through the resistance of a 1 K Ω is 124 μA (Figure 3.7). Just as seen in the plots for the voltage, the peak value of the current flowing the through the load when the load resistance connected is 100 Ωs (Figure 3.6) is less than the peak value when the value of resistance connected is 1 K-Ω (Figure 3.7). But the latter

decays quicker in comparison and attain values negligible with respect to the peak current value, hence they are represented on the plot by a flat line.

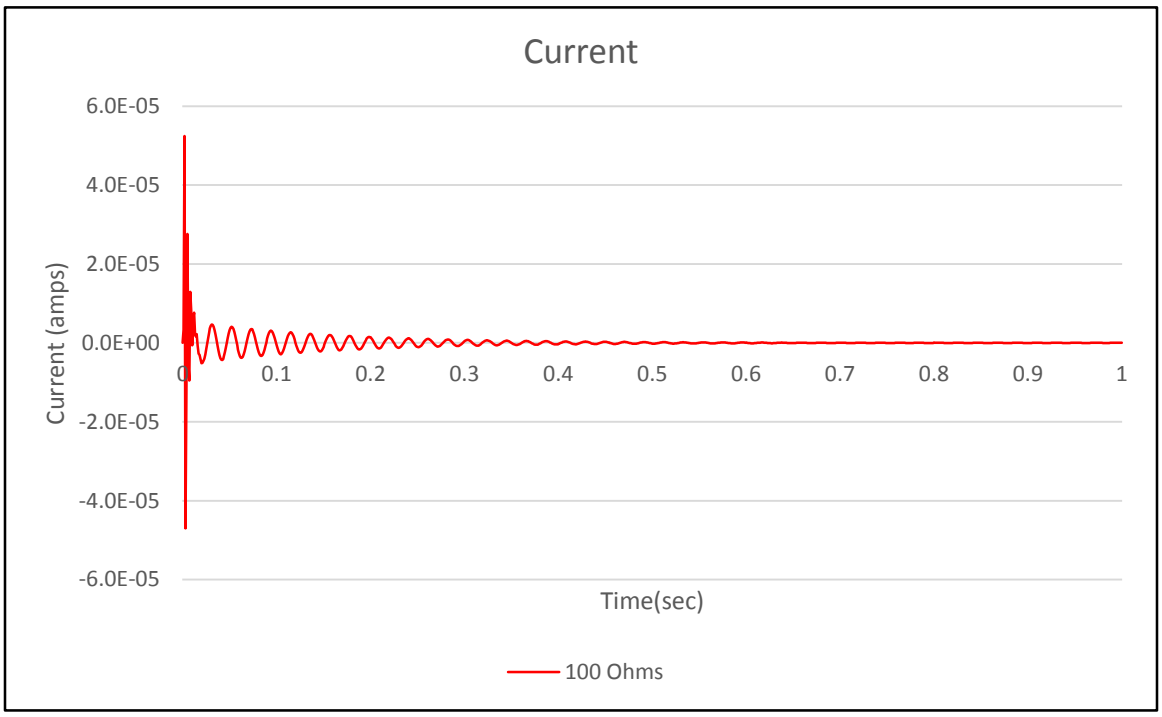

Figure 3.6: Current flowing through the current of 100 Ohms

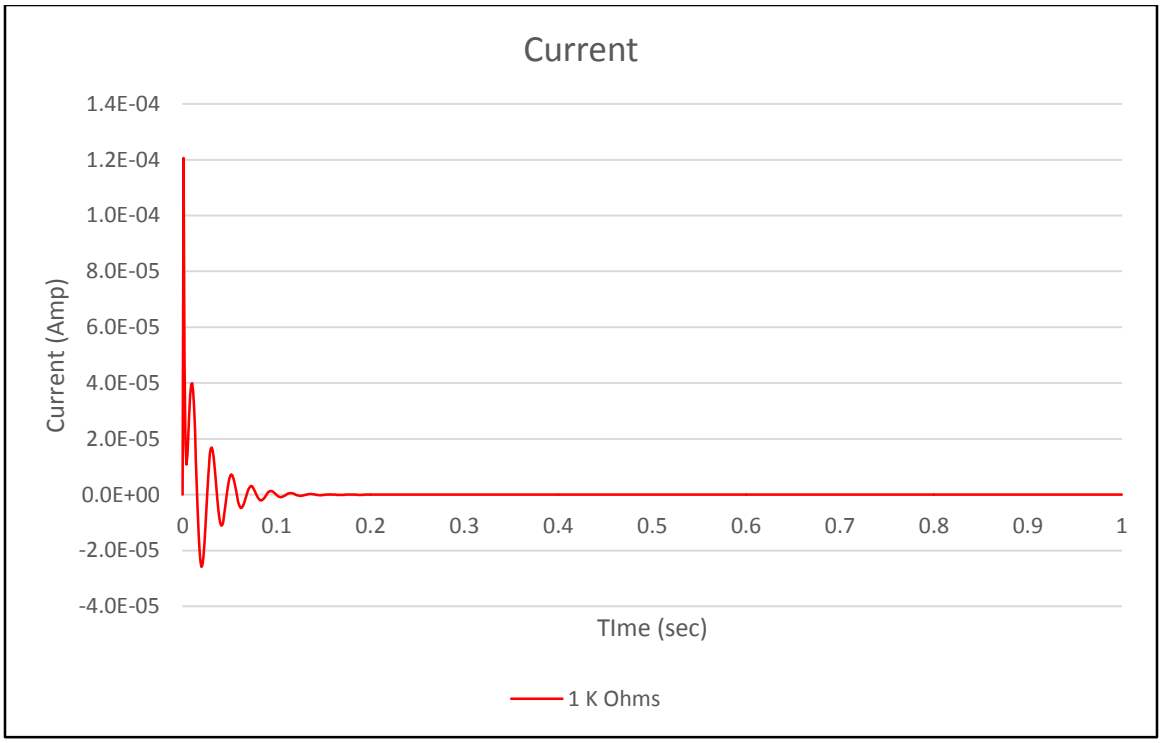

Figure 3.7: Current flowing through the current of 1 K Ohms

3.4 Instantaneous power generated across the load.

The instantaneous power generated power generated across the resistive load can thus be obtained as $P(t) = v^2(t)/R_L$. The instantaneous power generated for the load resistance of 100 Ωs and 1 K Ω are plotted as a function of time Figure 3.8 and Figure 3.9.

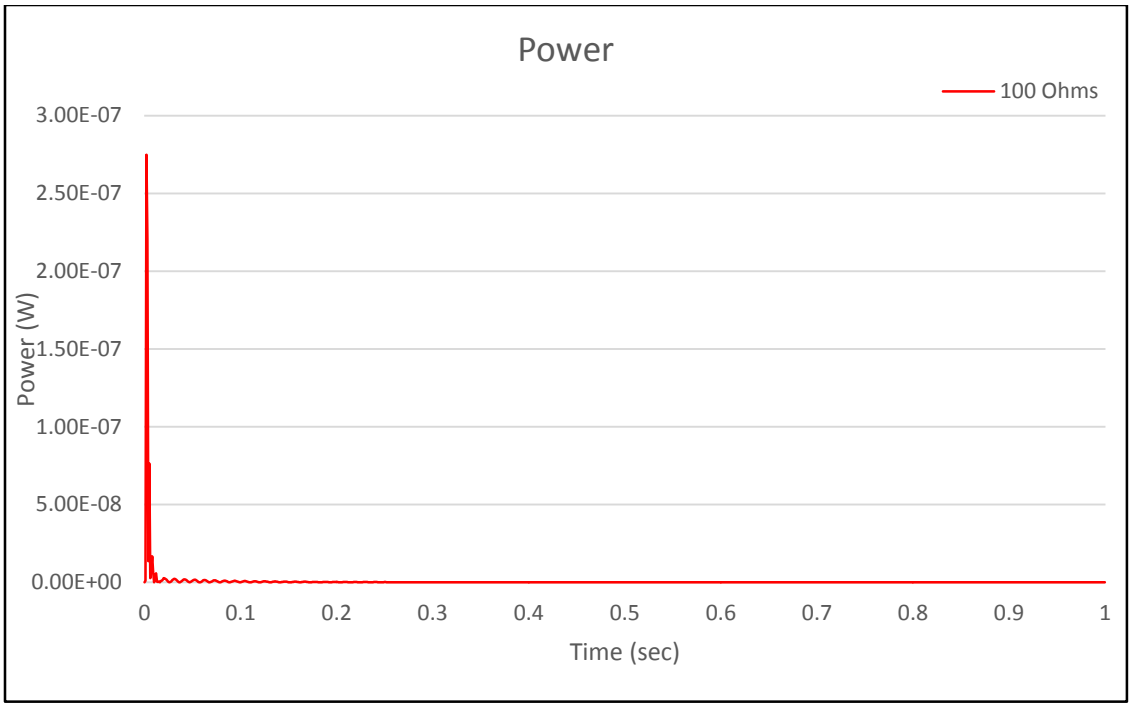

Figure 3.8: Power generated across a load resistance of 100 Ohms.

The maximum power generated by the unimorph cantilever when the connected to a resistance of 100 Ω s is 0.275μWs.

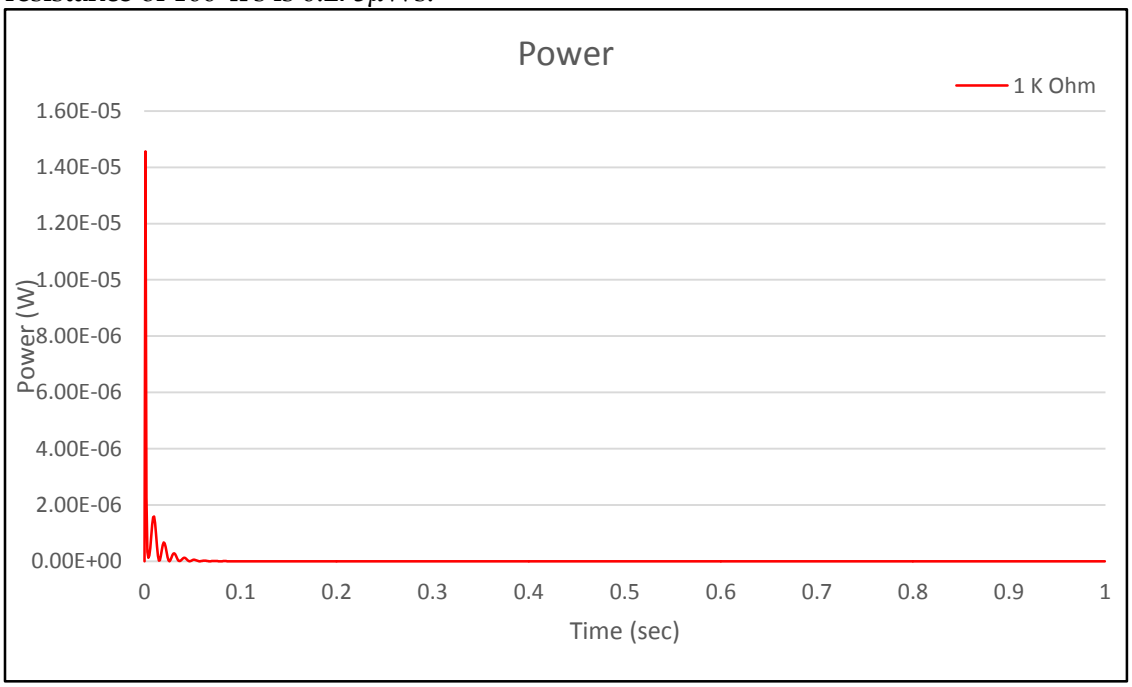

Figure 3.9: Power generated across a load resistance of 1 K Ohm.

The maximum power generated by the unimorph cantilever when the connected to a resistance of 1 KΩ is 14.6 μW. The unimorph can be connected to a circuit consisting rectifiers for post conditioning and connected to a secondary battery to harvest this power.

3.5 Efficiency calculations

The efficiency of a system is defined as the output obtained for the applied input. The efficiency for this system can be defined as the percentage of energy utilized from the applied impulse load.

$$H_{harvester} = \frac{electrical\ energy}{work\ done\ by\ applied\ force} \text{ x } 100, \tag{3.2}$$

The work done by the force applied to the beam is obtained by multiplying the magnitude of the force and the displacement.

$$work\ done = force \text{ x } displacement. \tag{3.3}$$

The magnitude of the impulse load acting on the beam is *0.01* and the corresponding displacement achieved due to this force is *13.4 mm*. The total work done by the impulse load is:

$$work\ done = 0.01 \text{ x } 13.4e-3 \text{ N-m},$$

$$= 1.34e-4.$$

The total energy generated by the harvester is obtained by integrating the area under the plot for instantaneous power. This is obtained by using the Matlab function *trapz()*. The energy generated in the harvester when a load resistance of 100 Ω is connected across the circuit is 0.7341 µW.

Substituting the values of the work done and electrical energy generated in equation (3.2),

$$H_{harvester} = \frac{0.7341\ e-06}{1.341\ e-04} \text{ x } 100 = 0.562\%$$

The harvester efficiency when the load resistance is 100 Ω is 0.562%.

The energy generated in the harvester when a load resistance of 1 KΩ is connected across the circuit is 325 µW.

Substituting the values of the work done and electrical energy generated in equation (3.2),

$$H_{harvester} = \frac{32.5\ e-06}{1.341\ e-04} \text{ x } 100 = 24.9\%$$

The harvester efficiency when the load resistance is 1KΩ is 24.9%.

From the discussion hitherto, it can be said that the current configuration of unimorph is suitable for resistances lower than 1 KΩ, due to the consistent voltage and current generation over extended period.

Typical micro sensors have power requirements ranging from 30μW to 150μW [49-51]. The impulse load acting on the beam can replicate the touch gesture as is applied on the present day touch screen devices. Touch screen devices have undergone vast development over the past decade [51] and it could be said that such device are subjected to incessant impulse load in the form of screen touches over the duration of its use. If the power generated by the unimorph harvester due to each such impulse load is harvested and stored it can be used to satisfy the power requirements mentioned for the sensors above.

Chapter 4

4. Conclusion and Future Work

4.1 Conclusions

In this thesis an analytical model for a cantilever unimorph beam was presented. The model was based on Euler-Bernoulli assumptions, where the internal strain-rate damping and external viscous damping were included for accuracy. The unimorph beam was excited by an impulse load acting on the free end of the cantilever beam. The impulse load was represented by a delta function. This work builds upon the analytical model for a piezoelectric unimorphs presented by Erturk A. and Inman D.[4], which is limited to solving problems involving harmonic loading expressed as an exponential function of the excitation frequency and time. In the present work, the analytical approach may be used to solve cantilevered beams subjected to non-harmonic force loading. This procedure can also be used to solve conventional problems such as the one solved in the work of Erturk A. and Inman D.[52].

The piezoelectric unimorph beam proposed in this thesis was modeled as an Euler-Bernoulli beam. Electromechanically coupled equations of motion were derived for the beam by applying Newton's second law of motion. The equations of motion are solved to obtain closed form solutions to predict the tip displacement, voltage generated across the load and power generated when the harvester was connected in series with a load

resistance. These de-coupled closed form solutions for response can be used for any cantilever unimorph which satisfy the assumptions for the Euler-Bernoulli beam theory.

A MATLAB script was written to solve the expressions mathematically for the known boundary conditions, loading conditions and electromechanical properties. Using MATALB, data sets of solutions for the tip displacement, voltage generated and power output are obtained. The data set generated for the tip displacement, voltage generated and power output are plotted as a function of time. The plot for tip displacement dampens exponentially, similar to the plot for tip displacement of a unimorph cantilever beam plotted in the work of Gao X. e*t. al. [12]*.

The voltage generated across the resistive load has been plotted as function of time. The peak values for the voltage increases with the increase in the load resistance value. But the exponential decay of the voltage increased with increase in the resistance.

The current flowing through the load resistance was plotted as a function of time. The maximum value of the current flowing through the resistor increases with increases the increase in the load resistance. But unlike the voltage generated the current remains with the range on microamperes. As the resistance increases the current production dampens down quickly.

The power generated across the load resistance due to each impulse load was plotted as a function of time. The value for the power generated were compared with the power requirements for modern micro-sensors. Hence it could be said that the particular

configuration for the unimorph harvester was suited for resistance values lower than 1 K-Ω as the voltage generation and current flow is consistent and continuous.

In summary, this model can be used for the prediction of the electrical response of the unimorph when subjected to a non-harmonic load. It can be used to move towards a generalized model which can predict the power output for forces that are not a function of frequency as well as conventional forces which have been previously studied in the works of Erturk A. [4]and Gao X. *et.al[12]*.

4.2 Future Work

The model presented in this thesis can further be developed for energy harvesting. Auxiliary components such as a circuit consisting of bridge rectifiers and capacitors are needed to regulate the voltage surges. The energy generated after condition the electrical output can be used to charge any secondary source of power. Also further investigations can be made to study the response of the beam when it is subjected to base motion excitation as well as impulse loading at the same time.

Touch gesture based technology is now present within a large extent of electronics like PDA, smart phones, car navigation systems, tablets, personal computers, user interfaces for industrial machines. The touch gesture by a person has been mathematically modeled as an impulse load acting in the model discussed before. Further research can be made regarding how this energy harvester can be used to tap the impulse created by the incessant touches and generate power to support micro-sensors within the electronics

circuit. The model discussed in the anterior can be developed to harvest energy from such touch gestures and other base excitations as well.

Appendix

MATLAB Code Script

The MATLAB script is as follows:

Hybrid Energy Systems Lab, Rutgers University, New Brunswick

```
%%Analytical model of a Cantilever Unimorph Beam under Impulse load
%%Presented by Abhinav Athavale
```

Under the guidance of Dr. Kimberly Cook-Chennault

```
clear;clc;        %clearing screen and previous variables
```

Defining Basic Parameters of the Unimorph Beam

Calculating the distances of the top and the bottom of the beam from the neutral axis

```
Y_p=66e+09;       %Youngs Modulus of PZT(GPa)
Y_s=100e+09;      %Youngs Modulus of Substrate(GPa)
t_p=0.4e-03;      %Thickness PZT(m)
t_s=0.5e-03;      %Thickness Substrate(m)
d_31=-190e-12;    %Dielectric constant(pm/V)
L=100e-03;        %Length of the beam(m)
Ro_p=7800;        %Density of PZT(kg/m^3)
Ro_s=7165;        %Density of Substrate(kg/m^3)
b=20e-03;         %Width of the Beam(m)

e_33=15.93e-09;   %permitivity in nano-Farad/meter
R_l= 1e+03;       %Load Resistance in Ohms
```

```
[Vu,YI,t_a,t_b,t_c,t_pc]=Upsilon(Y_p,Y_s,d_31, t_p,t_s,b); %Constant in the
governing differential and Bending Stiffness of the Beam
```

Calculating mass per unit length of the beam

```
m= b*(t_p*Ro_p+t_s*Ro_s);
```

Calculation of the spatial solution phi(x)

Calculating constants dependent on the spatial solution

```
Beta_L=roots_L;
Beta=Beta_L/L;
[phi,phi_diff,X_r, vphi_r]=constant(Beta_L,Beta,m,Vu,d_31,Y_p, t_pc, t_p,
e_33,L);
```

Calculating the natural and damped frequencies of first 4 modes using definition.

```
Xi=[0.01 0.013 0.033 0.064]; % Damping ratios according to paper
[w_r,w_d]= freq(Beta,YI,m,Xi); % Frequencies
freq_r=w_r/(2*pi);          % obtaining frequencies in Hz

%% Calculating Tau_c and roots to Laplace Equation
```

```
Tau_c=(R_l*e_33*b*L)/t_p; %calculating constant Tau_c
[p,r_1,r_2,r_3]=roots_c(Xi, w_r,w_d, X_r, vphi_r,Tau_c);
```

Calculating voltage generated.

Constants required P_y ,varphi, phi_L, w_d, Tau_c

```
P_y = -1e-02;              %magnitude of force.
t= 0:0.01:1;
[v,volt,A,B,C] = voltage(P_y, vphi_r, phi, w_d, Tau_c, r_1, r_2, r_3,t);
```

Calculating modal solution eta(t)

```
n_t=modes(P_y,Xi,w_r,w_d,t,A,B,C,r_1,r_2,r_3,X_r,vphi_r,phi,Tau_c);
```

Calculating displacement

```
w =summation(phi,n_t,t);
w=transpose(w);
```

Calculating power

```
pw= elec_power(v,R_l);
```

Plotting the expressions against time

```
plot(t,w);
title('Graph of Tip Displacement Vs Time')
xlabel('Time (sec)') % x-axis label
ylabel('Tip Displacement (m)') % y-axis label
pause(2);

plot(t,v);
title('Graph of Voltage Vs Time')
xlabel('Time (sec)') % x-axis label
ylabel('Voltage (V)') % y-axis label
pause(2);


plot(t,pw);
```

```
title('Graph of Power Vs Time')
xlabel('Time (sec)') % x-axis label
ylabel('Power (W)') % y-axis label

hold off;
% End of code
```

Function called to obtain Eigen Functions%%

```
function [z]= roots_L()

%Calculated the roots to characteristic root equation Equation (2.22)%
clear
f=@fun;
x0=1;
j=1;
z=zeros(1,4);
while and(x0<100,j<5)
    z(j)=fzero(f,x0);
    x0=x0+3;
    j=j+1;
end

end

function r= fun(x)
r=1+(cos(x)*cosh(x));
end
```

Function to calculate constants related to the natural frequencies

```
function[phi,phi_diff,X_r,vphi_r] = constant(Beta_L,Beta,m,Vu,d_31,Y_p, t_pc,
t_p, e_33,L)
```

Calculates Phi, d phi/dx ,X_r and returns to main.

```
B = zeros(1,length(Beta_L));
phi = zeros(1,length(Beta_L));
phi_diff = zeros(1,length(Beta_L));
vphi_r = zeros(1,length(Beta_L));

for k  = (1:length(Beta_L))

B(k)=(sinh(Beta_L(k))-sin(Beta_L(k)))/(cosh(Beta_L(k))+cos(Beta_L(k)));

phi(k)=sqrt(1/(m*L))*(cosh(Beta_L(k))-cos(Beta_L(k))-
B(k)*(sinh(Beta_L(k))-sin(Beta_L(k))));         % phi at x=L equivalent to
(2*sinh(Beta_L(k))*sin(Beta_L(k)))/(cosh(Beta_L(k))+cos(Beta_L(k)))

phi_diff(k)=sqrt(1/(m*L))*Beta(k)*(sinh(Beta_L(k))+sin(Beta_L(k))-
B(k)*(cosh(Beta_L(k))-cos(Beta_L(k))));         % phi` at x=L equivalent to
2*(sin(Beta_L(k))*cosh(Beta_L(k))+cos(Beta_L(k))*sinh(Beta_L(k)))/(cosh(Beta_L(
k))+cos(Beta_L(k)));

a=-(d_31*Y_p*t_pc*t_p)/(e_33*L);
vphi_r(k)=a*phi_diff(k);
end
X_r=Vu*phi_diff;

end
```

Calculating the natural and damped frequencies of first 4 modes using definition.

```
function [w_r,w_d] =freq(Beta,YI,m,Xi)
w_r=zeros(1,length(Beta));
w_d=zeros(1,length(Beta));
for k=(1:length(Beta))
w_r(k)=((Beta(k))^2*sqrt(YI/m)); %natural frequencies
w_d(k)=w_r(k)*sqrt(1-(Xi(k))^2); % corresponding damped frequencies
 end
end
```

Calculating roots to denominator of Equation (2.45)

```
function [r,r_1,r_2,r_3] = roots_c( Xi, w_r,w_d, X_r, vphi_r,Tau_c)
r=zeros(3,4);
p=zeros(1,4);
```

Calculating coefficients of the cubic equation.

```
for j=1:length(Xi)
    a=Tau_c;
    b=(2*Xi(j)*w_r(j)*Tau_c+1);
    c=(Tau_c*(w_r(j))^2+2*Xi(j)*w_r(j)+X_r(j)*vphi_r(j)*w_d(j)*Tau_c);
    d=(w_r(j))^2;
    p(j,:)=[a b c d];
end
```

Calculating roots from the coefficients

```
for j=1:length(Xi)
r(:,j)=roots(p(j,:));
end
% collecting roots in the sepearte tems
for j=1:1:3
    r_1=r(1,:);
    r_2=r(2,:);
    r_3=r(3,:);
 end
end
```

Calculating voltage generated.

Constants required P_y varphi phi_L w_d Tau_c

```
function [v,volt,A,B,C]= voltage(P_y, vphi_r, phi, w_d, Tau_c, r_1, r_2, r_3,t)
volt = zeros(length(vphi_r),length(t));
v = zeros(length(t),1);
A = zeros(1,length(vphi_r));
B = zeros(1,length(vphi_r));
C = zeros(1,length(vphi_r));
for k=1:length(r_1)
    A(k)= r_1(k)/((r_1(k)-r_2(k))*(r_1(k)-r_3(k)));
    B(k)= -r_2(k)/((r_1(k)-r_2(k))*(r_2(k)-r_3(k)));
    C(k)= r_3(k)/((r_1(k)-r_3(k))*(r_2(k)-r_3(k)));
    for j=1:length(t);
         volt(k,j)= P_y*vphi_r(k)*phi(k)* w_d(k)*Tau_c*...
             (
A(k)*exp(r_1(k)*t(j))+B(k)*exp(r_2(k)*t(j))+C(k)*exp(r_3(k)*t(j)));
    end
end
for k=1:length(t)
    v(k)= volt(1,k)+volt(2,k)+volt(3,k)+volt(4,k);

end
end
```

Calculating modal solution eta(t)

```
function n_t=modes(P_y,Xi,w_r,w_d,t,A,B,C,r_1,r_2,r_3,X_r,vphi_r,phi,Tau_c)
n_t=zeros(length(r_1),length(t));
for j=1:length(r_1)

A(j)=X_r(j)*P_y*vphi_r(j)*phi(j)*Tau_c*A(j)/((r_1(j))^2+2*Xi(j)*w_r(j)*r_1(j)+(
```

```
w_r(j))^2);

B(j)=X_r(j)*P_y*vphi_r(j)*phi(j)*Tau_c*B(j)/((r_2(j))^2+2*Xi(j)*w_r(j)*r_2(j)+(
w_r(j))^2);

C(j)=X_r(j)*P_y*vphi_r(j)*phi(j)*Tau_c*C(j)/((r_3(j))^2+2*Xi(j)*w_r(j)*r_3(j)+(
w_r(j))^2);
end


for j=1:length(r_1)
    for k=1:length(t)
        n_t(j,k)= (P_y*phi(j)*(exp(-
Xi(j)*w_r(j)*t(k)))*sin(w_d(j)*t(k))/w_d(j))...
           -A(j)*(w_d(j)*exp(r_1(j)*t(k))-exp(-
Xi(j)*w_r(j)*t(k))*(r_1(j)+Xi(j)*w_r(j))*sin(w_d(j)*t(k))-exp(-
xi(j)*w_r(j)*t(k))*(w_d(j)*cos(w_d(j)*t(k))))...
           -B(j)*(w_d(j)*exp(r_2(j)*t(k))-exp(-
Xi(j)*w_r(j)*t(k))*(r_2(j)+Xi(j)*w_r(j))*sin(w_d(j)*t(k))-exp(-
Xi(j)*w_r(j)*t(k))*(w_d(j)*cos(w_d(j)*t(k))))...
           -C(j)*(w_d(j)*exp(r_3(j)*t(k))-exp(-
Xi(j)*w_r(j)*t(k))*(r_3(j)+Xi(j)*w_r(j))*sin(w_d(j)*t(k))-exp(-
Xi(j)*w_r(j)*t(k))*(w_d(j)*cos(w_d(j)*t(k))));

    end
end
```

Calculating transverse displacement at x = L

```
function w =summation(phi,n_t,t)
w=zeros(1,length(t));
for k=1:length(t)
  w(k)= phi(1)*n_t(1,k)+phi(2)*n_t(2,k)+phi(3)*n_t(3,k)+phi(4)*n_t(4,k);
end
end
```

Calculating power

```
function pw = elec_power(v,R_l)
 pw=zeros(1,length(v));
for i=1:length(v)
    pw(i)=(v(i))^2;
end

pw=pw/R_l;
pw=transpose(pw);
end
```

Calculating harvester efficiency

```
elec_energy = trapz(pw);
mech_work = abs(P_y*max(w));
harv_eff=elec_energy*100/mech_work;
```

Plotting the expressions against time

```
plot(t,w);
title('Graph of Tip Displacement Vs Time')
xlabel('Time (sec)') % x-axis label
ylabel('Tip Displacement (m)') % y-axis label
pause(3);

plot(t,v);
title('Graph of Voltage Vs Time')
xlabel('Time (sec)') % x-axis label
ylabel('Voltage (V)') % y-axis label
pause(3);

plot(t,i_t);
title('Graph of Current Vs Time')
xlabel('Time (sec)') % x-axis label
```

```
ylabel('Current(Amp)') % y-axis label
pause(3);

plot(t,pw);
title('Graph of Power Vs Time')
xlabel('Time (sec)') % x-axis label
ylabel('Power (W)') % y-axis label

hold off;
%%End of code
```

Published with MATLAB® R2014a

References

1. Banerjee, S., *AN EXPERIMENTAL AND THEORETICAL ANALYSIS OF TWO AND THREE PHASE EPOXY BASED PIEZOELECTRIC COMPOSITES*, in *Mechanical and Aerospace Engineering*2013, Rutgers University: New Brunswick, NJ.
2. Cook-Chennault, K.A., N. Thambi, and A.M. Sastry, *Powering MEMS portable devices- a review of non-generative and generative power supply systems with special emphasis on piezoelctric energy harvesting system.* Smart Materials and Structures, 2008. **17**(4).
3. Gao, X., W.-H. Shih, and W.Y. Shih, *Induced voltage of piezoelectric unimorph cantilevers of different nonpiezoelectric/piezoelectric length ratios.* Smart Materials and Structures, 2009. **18**.
4. Erturk A., I.D.J., *A Distributed Parameter Electromechanical Model for Cantileverd Piezoelecrtric Energy Hareveter.* Jounal Of Vibrations and Accoustics, August 2008: p. Vol.130.
5. *QuickLogic Delivers First Smartphone and Wearable Sensor Hub With Under 150 Microwatt Active Power and Programmable Flexibility*. 2014 [cited 2014 09/03]; Available from: http://ir.quicklogic.com/releasedetail.cfm?releaseid=868853.
6. Hsieh, C.-T., et al. *Profile-driven program synthesis for evaluation of system power dissipation*. in *Proceedings of the 34th annual Design Automation Conference*. 1997. ACM.
7. *Design techniques for energy efficient*, in *Journal of Systems Architecture*. 2000.
8. Pedram, M. *Power optimization and management in embedded systems*. in *Proceedings of the 2001 Asia and South Pacific Design Automation Conference*. 2001. ACM.
9. Anton, S. and H. Sodano, *A review of power harvesting using piezoelectric materials (2003–2006)*, in *Smart Materials and Structure*2007, IOP Publishing.
10. Roundy, S., *On the Effectiveness of Vibration-based Energy Harvesting.* 2005. **16**(October).
11. Erturk, A., *Electromechanical modelling of Piezoelctric Energy Harvestors*, 2009.
12. Gao, X., W. Shih, and W.Y. Shih, *Induced voltage of piezoelectric unimorph cantilevers of different nonpiezoelectric/piezoelectric length ratios.* 2009. **18**.
13. Lumentut, M. and I. Howard, *Analytical and experimental comparisons of Electromechanical Vibration Response of a Piezoelectric Bimorph Beam for Power Harvesting.* Mechanical Systems and Signal Processing., 2011. **36**.
14. Abdelkefi, A., et al., *An energy harvester using piezoelectric cantilever beams undergoing coupled bending–torsion vibrations.* Smart Materials and Structures, 2010/2011. **10**.

15. Erturk, A. and D.J. Inman, *A Distributed Parameter Electromechanical Model for Cantileverd Piezoelecrtric Energy Hareveter.* Journal Of Vibrations and Accoustics, 2008. **130**(August 2008).

16. *Smartphone Users Worldwide Will Total 1.75 Billion in 2014*. 2014 [cited 2015 January, 20]; Mobile users pick up smartphones as they become more affordable, 3G and 4G networks advance - See more at: http://www.emarketer.com/Article/Smartphone-Users-Worldwide-Will-Total-175-Billion-2014/1010536#sthash.tI0U16nw.dpuf]. Available from: http://www.emarketer.com/Article/Smartphone-Users-Worldwide-Will-Total-175-Billion-2014/1010536.

17. Wikipedia. *Mobile operating system*. 2015 February 28, 2015 [cited 2015 March, 1]; Mobile operating system]. Available from: http://en.wikipedia.org/w/index.php?title=Mobile_operating_system&oldid=649242818.

18. Wikipedia. *Google Play*. 2015 February,27 2015 [cited 2015 March,1]; Android (operating system)]. Available from: http://en.wikipedia.org/wiki/Google_Play.

19. Wikipedia. *App Store (iOS)*. 2015 March,1 [cited 2015 March,1]; App Store (iOS)]. Available from: http://en.wikipedia.org/w/index.php?title=App_Store_(iOS)&action=history.

20. Erturk, A., , Inman, D., *Piezoelectric Energy Harvesting*. 2011: John Wiley and Sons, Ltd, Publications.

21. Starner, T. and J. Paradiso, *Human Generated Power for Mobile Electronics*, in *Low Power Electronics Design*. 2004, CRC Press Hall.

22. Moore, G.E., *Cramming more components onto integrated circuits.*

23. Cook-Chennault, K.A., N. Thambi, and A.M. Sastry, *Powering MEMS portable devices- a review of non-generative and generative power supply systems with special emphasis on piezoelctric energy harvesting system.* 2008. **17**(4).

24. *Piezoelectricity*, in *APC Intenational Ltd.*2014.

25. Arnau, A. and D. Soares, *Fundamentals of Piezoelectricity*, in *Piezoelctric Transducers and Application*. 2008, Springer Berlin Heidelberg,. p. 1-38.

26. Glynne-Jones, P., et al., *An electromagnetic, vibration-powered generator for intelligent sensor systems.* Sensors and Actuators, 2004. **A**(110): p. 344-349.

27. Mitcheson, P., et al., *MEMS electrostatic micropower generator for low frequency operation.* Sensors and Actuators, 2004. **A**(115): p. 523-529.

28. Kornbluh, R., et al., *Electroelastomers: Applications of Dielectric Elastomer Transducers for Actuation, Generation and Smart Structures.* Smart Structures and Materials, 2002. **4698**: p. 254-270.

29. Roundy, S., P. Wright, and J. Rabaey, *A study of low level vibrations as a power source for wireless sensor nodes.* Computer Communications. , 2003. **26**.

30. IEEE. *An American National Standard IEEE Standard on Piezoelectricity*. 1987. New York: IEEE.
31. Bottega, W., *Engineering Vibrations*. 1 ed. 2006: CRC Press.
32. Abdelkefi, A., et al., *An energy harvester using piezoelectric cantilever beams undergoing coupled bending–torsion vibrations.* 2010/2011. **10**.
33. Neiss, S., et al., *Analytical model for nonlinear piezoelectric energy harvesting devices.* Smart Materials and Structures. **23**(10).
34. Wang, W.-C., et al., *Acoustic energy harvesting by piezoelectric curved beams in the cavity of a sonic crystal.* Smart Materials and Structures, 2010. **19**(4): p. 045016.
35. Mo, C., J. Davidson, and W. Clarke *Energy harvesting with piezoelectric circular membrane under pressure loading.* Smart Materials and Structures, 2014. **23**(4): p. 45005.
36. Aridogan, U., I. Basodgan, and A. Erturk, *Analytical modeling and experimental validation of a structurally integrated piezoelectric energy harvester on a thin plate.* Smart Materials and Structures, 2014. **23**(4): p. 39-45.
37. Lumentut, M. and I. Howard, *Analytical andexperimentalcomparisonsof.* 2011. **36**.
38. Yuan, Y., et al., *Analytical solutions to flexural vibration of slender piezoelectric multilayer cantilevers.* Smart Materials and Structures, 2014. **23**(9).
39. Hosseini, S., et al., *Analytical solution for nonlinear forced response of a viscoelastic piezoelectric cantilever beam resting on a nonlinear elastic foundation to an external harmonic excitation.* Composites Part B: Engineering. **67**: p. 464-471.
40. Umeda M., N.K., Ueha S., *Analysis of the Transformation of Mechanical Impact Energy to Electric Energy Using Piezoelectric Vibrator.* Japanese Journal of Applied Science, 1996(35): p. 3267-73.
41. M., P., *Impulse excitation of piezoelectric bimorphs for energy harvesting: a dimensionless model.* Smart Materials and Structures, 2014. **23**(4).
42. Benaroya, H. and M.L. Nagurka, *Mechanical Vibration: Analysis, Uncertanities, and Control.* 2009: CRC Press.
43. Hibbler, R.C., *Mechanics of Materials*. Sixth ed. 2004: Prentice Hall.
44. Hibbler, R.C., *Mechanics of Material*. 2004: Prentice Hall.
45. A Erturk, D.J.I., *A Distributed Parameter Electromechanical Model for Cantileverd Piezoelecrtric Energy Hareveter.* Journal Of Vibrations and Accoustics, August 2008. **130**(August 2008).
46. Baruh, H., *Analytical Dynamics*. 1999: WCB/McGraw-Hill
47. Banks , H.T. and D.J. Inman *On Bending Mechanism in Beams.* 1991. **Vol. 58**.
48. Whitney, S. *Vibrations of Cantilever Beams: Deflection, Frequency, and Research Uses* 1999 [cited 2015 February 3]; Available from: http://emweb.unl.edu/Mechanics-Pages/Scott-Whitney/325hweb/Beams.htm.

49. S.W. Arms, C.P.T., D.L. Churchill, J.H. Galbreath, S.W. Mundell, *Power Management for Energy Harvesting Wireless Sensors.* SPIE Int'l Symposium on Smart Structures & Smart Materials 2005.

50. N. Massari, M.G., S. A. Jawed, G. Soncini, *A 100 Microwatt Ultra Low-Power Contrast-Based Asynchronous Vision Sensor*, in *Sensors and Microsystems*. 2010, Springer Netherlands.

51. *QuickLogic Delivers First Smartphone and Wearable Sensor Hub With Under 150 Microwatt Active Power and Programmable Flexibility*, 2014, Acquire Media.

52. Erturk, A. and D. Inman, *Piezoelectric Energy Harvesting*. 2011: John Wiley and Sons, Ltd, Publications.